Universidade de Aveiro
2021

Diogo Filipe Pires Marinheiro

Desenvolvimento de Nanoconjugados de Sílica Mesoporosa com Nutracêuticos

Design of Nutraceutical–Mesoporous Silica Nanoconjugates

Universidade de Aveiro Departamento de Química

2021

Diogo Filipe Pires Marinheiro

Desenvolvimento de Nanoconjugados de Sílica Mesoporosa com Nutracêuticos

Design of Nutraceutical–Mesoporous Silica Nanoconjugates

Dissertação apresentada à Universidade de Aveiro para cumprimento dos requisitos necessários à obtenção do grau de Mestre em Biotecnologia (ramo Alimentar), realizada sob a orientação científica da Doutora Bárbara Leite Ferreira, Investigadora do CICECO/Departamento de Química da Universidade de Aveiro, e da Doutora Ana Luísa Daniel da Silva, Investigadora Auxiliar do CICECO/Departamento de Química da Universidade de Aveiro.

o júri

presidente

Doutora Cláudia Sofia Cordeiro Nunes
Investigadora do CICECO/Departamento de Química da Universidade de Aveiro

Doutora Bárbara Joana Martins Leite Ferreira (Orientadora)
Investigadora do CICECO/Departamento de Química da Universidade de Aveiro

Doutora Márcia Carvalho Neves
Investigadora Auxiliar do CICECO/Departamento de Química da Universidade de Aveiro

agradecimentos

Em primeiro lugar quero deixar um especial agradecimento às minhas orientadoras que foram incansáveis, sempre o mais prestáveis e dedicadas possível mesmo nas circunstâncias mais apertadas. Doutora Bárbara Ferreira por me guiar neste trajeto, não só com a sua orientação científica, mas com todo o apoio e ajuda, pela motivação que sempre me deu ao longo deste ano difícil, pela paciência, por todo o tempo que dedicou a mim e a este trabalho, sempre disponível a todo o momento para tudo o que pudesse precisar. Para além de uma excelente profissional com um talento inato para a orientação, foi para mim um excelente ser humano que tive o prazer de conhecer e trabalhar com, marcou-me enquanto estudante e marcará sem dúvida a minha vida. Doutora Ana Luísa por partilhar comigo o seu conhecimento, pela paciência e atenção, sempre cordial e de uma simpatia ímpar, foi crucial para o desenvolvimento deste trabalho. A elas o meu profundo e sincero obrigado.

A todos os técnicos que realizaram algumas das análises experimentais aqui discutidas ou de alguma forma me ajudaram. Eng. Celeste Azevedo que realizou as análises de Termogravimetria, bem como prestou auxílio nas técnicas de espectroscopia de IR e UV-vis. Eng. Célia Miranda que realizou as várias análises de BET. Dra. Marta Ferro que adquiriu as imagens de microscopia. Um agradecimento especial à Dona Manuela Marques pela aquisição dos dados relativos à Análise Elementar, e também pela disponibilidade para as inúmeras pesagens necessárias. Aos colegas de laboratório e do Departamento de Química que sempre se mostraram disponíveis para me ajudar e esclarecer. Mestre Carlos Bornes pela prestabilidade e ajuda. Muito obrigado à Dra. Isabel Vieira e ao Dr. Ismael Domingos por disponibilizarem material fundamental ao exercício deste trabalho.

Um muito obrigado do fundo do coração à minha família e amigos por todo o apoio sobretudo nos momentos mais difíceis. O último e mais especial agradecimento, aos meus pais, o esforço que fizeram ao longo destes anos para eu poder chegar aqui, é para mim uma inspiração que me dá força para continuar.

palavras-chave

Resveratrol, nutracêuticos, nanoparticulas de silica mesoporosas, nanotecnologia, biodisponibilidade

resumo

O resveratrol (RSV) é um nutracêutico naturalmente presente em diversos alimentos como o vinho tinto, casca de uva, amendoim entre outros. Possui propriedades benéficas para a saúde humana como atividade antioxidante, anti-inflamatória e anticancerígena, entre outras. Porém, devido às características físico-químicas que apresenta, principalmente baixa solubilidade em água e biodisponibilidade, a sua aplicabilidade é limitada. Nos últimos anos, para contornar estas limitações têm sido desenvolvidas abordagens baseadas em nanotransportadores. Este trabalho apresenta os resultados da síntese e caracterização de nanopartículas de sílica mesoporosas (MSNs) e avalia a sua capacidade de encapsular e libertar, em condições *in vitro*, o RSV. Com este propósito foram estudadas várias condições de síntese e dois métodos de carregamento foram testados, por imersão e evaporação. O último mostrou ser mais eficaz permitindo carregamentos mais elevados. Os estudos de libertação *in vitro* sugerem um aumento da solubilidade em água do RSV encapsulado, relativamente à sua forma livre, bem como uma libertação mais rápida em meio ácido.

keywords

Resveratrol, nutraceuticals, mesoporous silica nanoparticles, nanotechnology, bioavailability

abstract

Resveratrol (RSV) is a nutraceutical naturally present in various foods such as red wine, grape skins, peanuts, among many others. This compound has beneficial properties for human health such as antioxidant, anti-inflammatory and anticancer activities, among others. However, due to is physicochemical characteristics, mainly its low solubility in water that results in low bioavailability, the applicability of this compound is limited. In order to overcome these limitations, nanocarriers based approaches have emerged in the last years. The present work shows the results of the synthesis and characterization of mesoporous silica nanoparticles (MSNs) and evaluates their capacity to encapsulate and in vitro release RSV. With this purpose several synthesis conditions were investigated and two RSV loading methods were tested, by immersion and evaporation. The latter proved to be more effective allowing higher loads. The in vitro release studies suggest an increase in water solubility of the encapsulated RSV, when compared to the free one, and a faster release in acidic medium.

Abbreviatures

BBB	Blood-brain barrier
BET	Brunauer-Emmet-Teller
BHJ	Barret, Joyner and Halenda
CTAB	Cetyltrimethylammonium bromide
CTAC	Cetyltrimethylammonium chloride
DSC	Differential Scanning Calorimetry
DLS	Dynamic Light Scattering
FDA	Food and Drugs Administration
FTIR	Fourier-Transform Infrared
GI	Gastrointestinal
GIT	Gastrointestinal tract
GRAS	Generally Recognized as Safe
MHSNs	Mesoporous Hollow Silica Nanoparticles
MSNs	Mesoporous Silica Nanoparticles
NPs	Nanoparticles
PBS	Phosphate buffered saline

PEG	Polyethylene glycol
PLA	Poly(D, L-lactic acid)
RSV	Resveratrol
SEM	Scanning Electron Microscope
siRNAs	Small interference RNA
STEM	Scanning Transmission Electron Microscope
TEA	Triethanolamine
TEM	Transmission Electron Microscope
TEOS	Tetraethyl orthosilicate
TGA	Thermogravimetric Analysis
XRD	X-ray Diffraction

Figure index

Table Index

Contents

I. Introduction

1. Nutraceuticals

"Let food be thy medicine and medicine be thy food" these phrase from Hippocrates is gaining greater attention by the scientific community in the last years [1]. Following this idea, the interest in nutraceuticals is growing, they are any foods and food constituents that provide health benefits beyond basic nutrition, including the prevention and treatment of disease. Dietary consumption of nutraceuticals may be associated with decreased risks of multiple chronic diseases [2]. The term nutraceutical was first proposed by Stephen L. DeFelice in 1989 and it results from the combination of the words "nutrition" and "pharmaceutical". These bioactive compounds are structurally and functionally diverse and include numerous agents such as phenolic compounds, carotenoids, vitamins, dietary fiber, probiotics, prebiotics and fatty acids [1].

Pleiotropic effects and relatively nontoxic behavior make nutraceuticals an interesting subject in the area of cancer research, for example, many nutraceuticals have been investigated for cancer prevention. They may also prevent the progression of cancer [1]. For example, it was found that lycopene, a nutraceutical present in tomatoes, decreases by 31% pancreatic cancer risk among men and that tomato-based products with high levels of lycopene could reduce pancreatic cancer risk [3]. The strategy of combinate chemotherapeutic drugs with nutraceutical in a single nanocarrier has been investigated due to its potential killing cancer cells while preventing the toxicity towards normal cells, this concept of selective death is known as "magic bullet" [1].

Despite the health benefits of nutraceuticals their clinical efficacy is limited due to poor aqueous solubility and poor permeability which leads to poor bioavailability. Other physicochemical and physiological processes may also contribute for poor bioavailability of nutraceuticals such as restricted release from the food matrix, chemical instability, formation of insoluble complexes with other components in the gastrointestinal tract (GIT), biotransformations in the GIT, slow absorption from the GIT and first-pass metabolism [1],

[2]. The oral bioavailability of a nutraceutical is defined as the fraction ingested that reaches the systemic circulation in an active form becoming available to be distributed to the tissues and organs [2]. In order to counteract these phenomena, scientific community has focused his interest in developing nanocarriers based delivery of nutraceuticals strategies, enhancing bioavailability and efficacy, and protecting them from adverse gastrointestinal conditions. Nanoparticles (NPs) can be designed to help nutraceuticals skip first-pass metabolism in which nutraceuticals are metabolized in the gut and liver [1], [2]. In this field different kinds of nanocarriers have been explored and are discussed further down this chapter. A classification system called Nutraceutical Biopharmaceutical Classification Scheme (NuBACS) has been introduced to characterize the main factors limiting the oral bioavailability of nutraceutical, this system is analogous to the Biopharmaceutical Classification System (BCS) [4].

2. Resveratrol

Resveratrol (3,5,4′-trihydroxystilbene, RSV) [5] is a naturally occurring polyphenol and phytoalexin, which is produced by plants in response to environmental stress such as fungal infections, injury and UV radiation [6]. It can be found in skin and seeds of more than 70 different plant species, including many foods commonly consumed in the human diet such as grapes (also present in red wine), berries, grains, tea, and peanuts [7]. Despite the fact that RSV has been more associated with red wine, it is also consumed as a non-alcoholic dietary supplement sold in pill or liquid forms. In 2012, the estimated global market for RSV was US$ 50 million [8].

It is a Biopharmaceutics Classification System (BCS) class II drug with poor aqueous solubility (0.03 g/L) and a partition coefficient (log Po/w) of 3.1. RSV exists in two geometric isomers, *cis*- and *trans*-, as shown in the Figure 1 with the latter being more abundant and biologically active [6], which gives trans-RSV the recognition as the bioactive form of RSV, cis-RSV is kown to be more susceptible to light-induced isomerization and auto-oxidation [9]. The chemical structure of RSV is similar to the estrogen diethylstilbestrol, with two phenol rings linked by a styrene double bond generating 3,4,5-trihydroxystilbene. The *trans*-isomer can be transformed into the *cis*- form under UV radiation exposure. *Trans*-RSV is commercially available and is relatively stable if protected

from high pH and light [10]. Once is a highly photosensitive compound susceptible to UV-induced isomerization, more than 80% of the *trans*-RSV in solution is converted to *cis*-RSV if exposed to light for 1 h [11]. Its molecular formula is $C_{14}H_{12}O_3$ and presents a molecular weight of 228.247 g mol^{-1}. The three –OH groups linked to the aromatic rings in RSV chemical structure, make it prone to further modifications, which result in several different active RSV derivatives, being pterostilbene one of the most common [9].

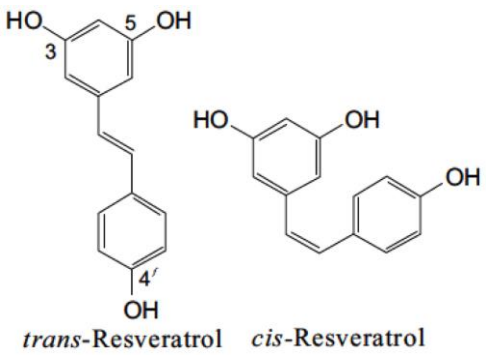

Figure 1 – RSV trans- and cis-isomers. Adapted [7].

The solubility of RSV in water is very low (ca. 0.13 mM) [9]. The solubility of trans-RSV in ethanol + water mixtures increase with increasing mole fraction of ethanol, whereas the solubility curve (the solubilities vs the mole fraction of acetone on solute-free basis) of an acetone + water mixed system presents a maximum. The solubilities of trans-RSV in both mixture systems increase with increasing temperature [12].

RSV is well known for its antioxidant, anti-inflammatory, cardio-protective, and neuro-protective properties, and has shown its potential in treatment of various disorders mediated by free radicals and oxidative stress [5], [6], metabolic disorders [13] and has also demonstrated a strong anti-cancer activity [6], [13], [14]. Additionally trans-RSV is well tolerated by humans since a 450 mg/day dose of RSV can represent a safe dose for a 70 kg individual [11]. At least 110 clinical trials are or have been performed with RSV, these trials have been made for many different diseases like: aging, cardiovascular disorders, cancer, neurodegenerative, obesity among others [8]. The interest in RSV emerged from some epidemiological studies that correlated red wine consumption to the low incidence of cardiovascular diseases in French population, a phenomenon known as the ‘‘French Paradox’’. The incidence of heart infarction in this population is about 40% lower than in

the rest of Europe. It was proposed that the phenolic compounds could be responsible for the beneficial properties of red wine, RSV, as a phenolic component of red wine, was thought to be responsible for these pointed benefits [11]. However, RSV suffer from many pharmacokinetic limitations like short biological half-life, chemical instability due to its tendency to suffer oxidation and extreme photosensitivity, its extensive and rapid metabolism and elimination, low aqueous solubility and poor bioavailability, representing a hindrance to its clinical utility [11], [14]. To overcome this challenge, RSV was incorporated into different nano-formulations to enhance its solubility and bioavailability [14].

Whilst the oral absorption of RSV in humans is high (~75%), the drug bioavailability is less than 1% as a result of erratic absorption in the gut and extensive first pass metabolism in the intestine and liver [6]. Upon administration, it is quickly and extensively metabolized in the body [15]. Access to the central nervous system (CNS) is limited by the blood–brain barrier (BBB), which is formed by tight junctions between brain endothelial cells, that protects the CNS from variations in blood composition and toxins and consequently restricts the penetration of various drugs [5]. Therefore it seems desirable to stabilize RSV to preserve its biological and pharmacological activities and enhance its bioavailability [11].

3. Nanoparticles as nutraceutical carriers

3.1. An overview

Nanotechnology is the science of engineering materials and systems on a molecular scale, usually less than 100 nanometers [16], and has evolved as the principal component of science in the current century [17]. It consists in the development of diverse organic and inorganic nanomaterials, using diverse inorganic and organic components including phospholipids, lactic acid, chitosan, dextran, polyethylene glycol (PEG), cholesterol, carbon, silica, and some metals [18]. Nanotechnology has various fields of application, for instance in fiber and textiles, agriculture, electronics, forensic science, space, medical therapeutics [19], antimicrobial applications [20], and food industry [21]. NPs are wide class of materials that include particulate substances, which have one dimension less than 100 nm at least [22], with a crystalline or an amorphous structure that possess unique physical and chemical

properties that differ from those displayed by either isolated atoms or bulk materials. NPs size may vary in a range of between 1 and 100 nm, which is similar to the size of many vital biomolecules such as antibodies, membrane receptors, nucleic acids, and proteins. These mimicking size features, together with their high surface area to volume ratio, make NPs a powerful tool in modern nanomedicine [23].

The small size of NPs endows them with remarkable physicochemical properties for numerous novel applications [21]. Features like high surface-to-volume ratio, nanoscale size, and favorable physicochemical characteristics make NPs suitable vehicles for drug delivery. These nanocarriers enhances aqueous solubility, extends shelf life, protects the food components against moisture, enables controlled release, influence texture, and flavor. Further, nanocarriers can modulate pharmacodynamic as well as pharmacokinetic profiles of nutraceuticals [1], enhancing the efficacy of nutraceuticals through encapsulation, protection and/or controlled release [2]. An example of this is use of nanoliposomes, a type of NP, to protect (-)-epigallocatechin gallate, a green tea polyphenol, from adverse gastrointestinal (GI) conditions [24].

NPs-based therapeutics have shown to be promising due to the flexibility in designing and modifying their compositions and structures for enhanced bioavailability and delivery efficiency, as well as site specific targeting [5]. The success of NPs as therapeutics carriers for various drugs can be associated to unique properties like higher therapeutic efficacy, lower toxicity and the ability to encapsulate and deliver poorly soluble drugs [18]. NPs have led to an exponential increase in the reactivity at both cellular and molecular levels. The unique behavior of NPs in terms of cellular endocytosis, transcytosis, neuronal and circulatory translocation and distribution, may also be associated with potential toxicity. In this area efforts have been made to optimize the methodology applied to nanotoxicology [23].

There are a few types of NPs used for delivery of nutraceuticals. Based on their constitution these nanocarriers can be broadly classified into three categories: polymeric nanocarriers, lipid-based nanocarriers and inorganic nanocarriers (Figure 2) [1].

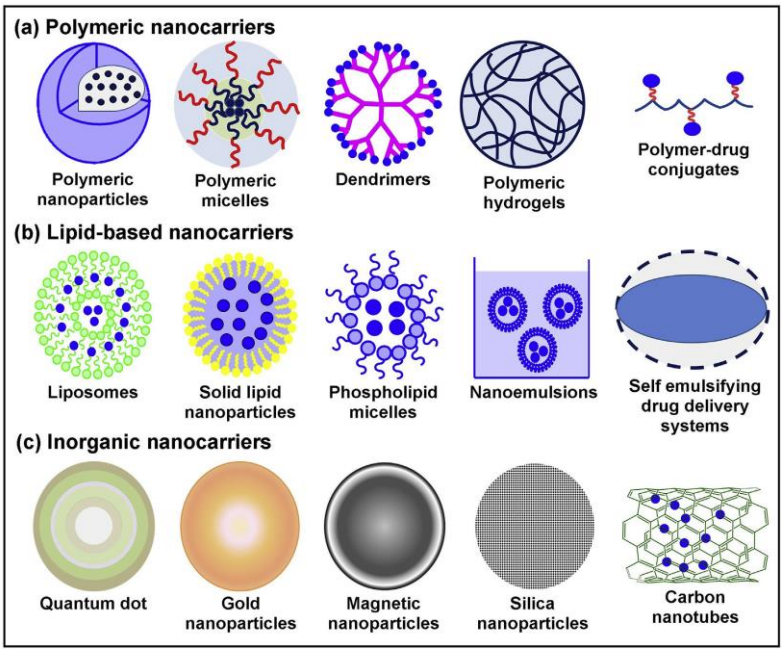

Figure 2 – Types of NPs used for nutraceuticals delivery [1].

Various non-biodegradable and biodegradable biocompatible polymeric nanocarriers have been exploited for nutraceutical delivery such as poly(D,L lactic-co-glycolic acid) (PLGA), poly (D, L-lactic acid) (PLA), poly(ethylene glycol) (PEG), poly(Ɛcaprolactone) (PCL) [18], [19], among others such as polysaccharides based polymers such as chitosan, starch, cellulose, alginate, pectin, etc [1], [18]. These polymeric delivery systems have several advantages such as ease of surface modification and pH- dependent controlled release [1]. Furthermore, some of these polysaccharides have been approved by FDA (Food and Drug Administration) and attained GRAS (generally recognized as safe) status [20], including some of them approved as food additives [25].

Lipid-based drug delivery systems such as solid lipid NPs, liposomes, nanoemulsions, self-emulsifying systems have been used for enhancing the bioavailability and efficacy of nutraceuticals [1], including RSV [26], [27].

Inorganic nanocarriers for nutraceutical delivery include quantum dots, gold NPs, magnetic nanomaterials, silica NPs or nanosilica and carbon nanotubes. These nanocarriers have been used owing to their unique physiochemical properties, such as size, shape, chemical composition, higher surface to volume ratios and ability for surface functionalization [1].

Nanocarriers may be distinguished into monofunctional or multifunctional NPs, whereas monofunctional NPs have a single feature, for example, they may transport the drug to the tissue but will not be able to distinguish between healthy and unhealthy cells. On the other hand multifunctional NPs combine different functionalities, for example, transport and specific targeting [23].

3.2. Mesoporous Silica Nanoparticles – MSNs

Mesoporous silica-based materials were first reported in the early 1990s by Mobil Company [28]. Mesoporous silica nanoparticles (MSNs) are highly attractive for drug delivery due to their well-defined and controllable microstructure and excellent biocompatibility [5]. The superior chemical, mechanical and textural stability, and textural properties of MSNs such as exceptionally large surface area and pore volume and tunable pore sizes, provide greater capacity for drug loading and surface functionalization [5], [29], [30]. The great flexibility in surface functionality of MSNs is owned by the silanol groups (-Si-OH) available for modification [29]. All this provides superior cargo loading capacities to MSNs [30].

Nanosuspensions and orally delivered tablets of MSNs were successfully prepared, showing the applicability of MSNs in multiple dosage forms. It was proposed that these NPs can be used both intravenously as nanosuspensions or orally by forming tablets [6].

Mesoporous materials are defined as the one having a pore size in the range of 2–50 nm [17], although typical pore diameters are between 2 and 5 nm, with different sizes from nanoscale to microscale range, with large surface area (from 700 to 1000 m^2/g), pore volume (from 0.6 to 1 cm^3/g) [31] and an ordered arrangement of pores giving an ordered structure to it. The pore size of these could be varied and tuned through the choice of surfactants used in the synthesis of MSNs [17].

Varying the starting precursors and reaction conditions different MSNs with distinct properties can be synthesized, some examples are represented in Figure 3. Of these, MCM-41 and SBA-15 have been widely employed for drug delivery. They present a pore size between 1.5 nm to 8 nm and 5 nm to 9 nm respectively, and pore volume >1.0 cm^3/g and 1.17 cm^3/g respectively for MCM-41 and SBA-15. Another interesting feature of SBA-15 is there thick walls from 3.5 to 5.3 nm. These MSNs may vary in their pore size and/or

structural arrangement that may be cubic (KIT-5), lamellar (MCM-50) or hexagonal (MCM-41/SBA-15) [17], [32].

Synthesis of MSNs is based on the Stöber synthesis method that was developed for the preparation of non-porous silica, and that has been suffering modifications over the years. The synthesis can be achieved in acid, neutral or basic conditions. Depending on the reaction parameters used in the synthesis of many different particles may be synthetized, with different sizes, shapes and arrangements. Once the loading capacity is enhanced by large pore volume and, for drug delivery, the particle size must be uniform, these features must be ensured controlling reaction parameters such as pH, temperature, concentration and type of surfactant as well as the silica source. The synthesis occurs using three main components: a silica precursor (examples are: TEOS – tetraethyl orthosilicate, TMOS – tetramethyl orthosilicate, TMVS – tetramethoxyvinylsilane, THEOS – meta-silicate, sodium meta-silicate and THEOS - tetrakis(2-hydroxyethyl) orthosilicate), a non-ionic or cationic surfactant as a structure directing agent and a catalyst [17].

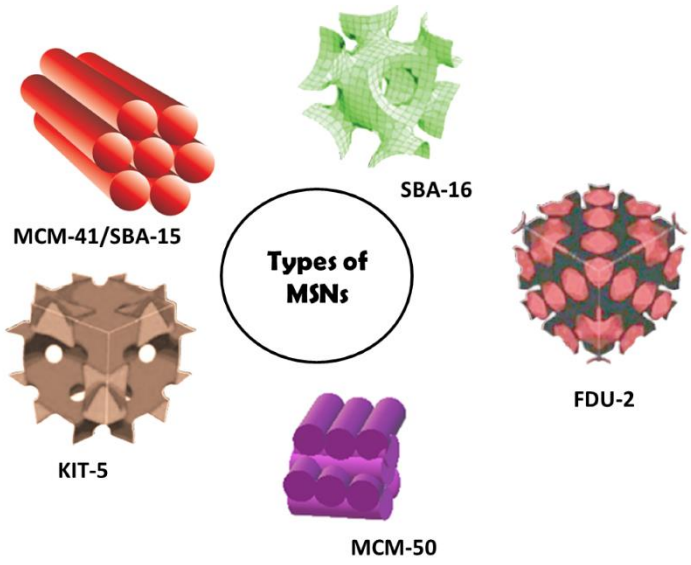

Figure 3 - Different types of MSNs with different arrangements [17].

A variety of sol−gel processes, a modified Stober's method [17], have been developed to synthesize meso-structured silica materials with highly tunable properties and morphologies from surfactant templates including parallel hexagonal mesochannels, radially oriented mesopores and hierarchical mesostructures [33]. Sol-gel process are widely used to

synthetize many inorganic materials. It involves a reaction in which alkoxide monomers are hydrolyzed and condensated into a colloidal solution (sol) that is a precursor to the formation of a network of polymer or discrete particles (gel). Multiple condensation results in a chain-like structure in the sol and network-like structure in gel form, this reaction is represented in *Equation 1*. In order to obtain de desired features of the MSNs and so enhance their properties, different procedures of the sol-gel process may be used [17].

$$\equiv Si - OH + RO - Si \equiv \leftrightarrow \equiv Si - O - Si \equiv + ROH$$

Equation 1 – Reaction of condensation of the alkoxide monomers. R may be a hydrogen atom or a substituent group such as methyl, ethyl, propyl, butyl, etc. [17].

The synthesis of MSNs may occur by liquid crystal template mechanism in which hydrolysis and condensation of the silica precursor (e.g. TEOS) to form solid silica takes place on the surface of surfactant micelles, as shown in

Figure 4. In this method the silica network gets built throughout the liquid–crystalline phases of non-ionic surfactants [17].

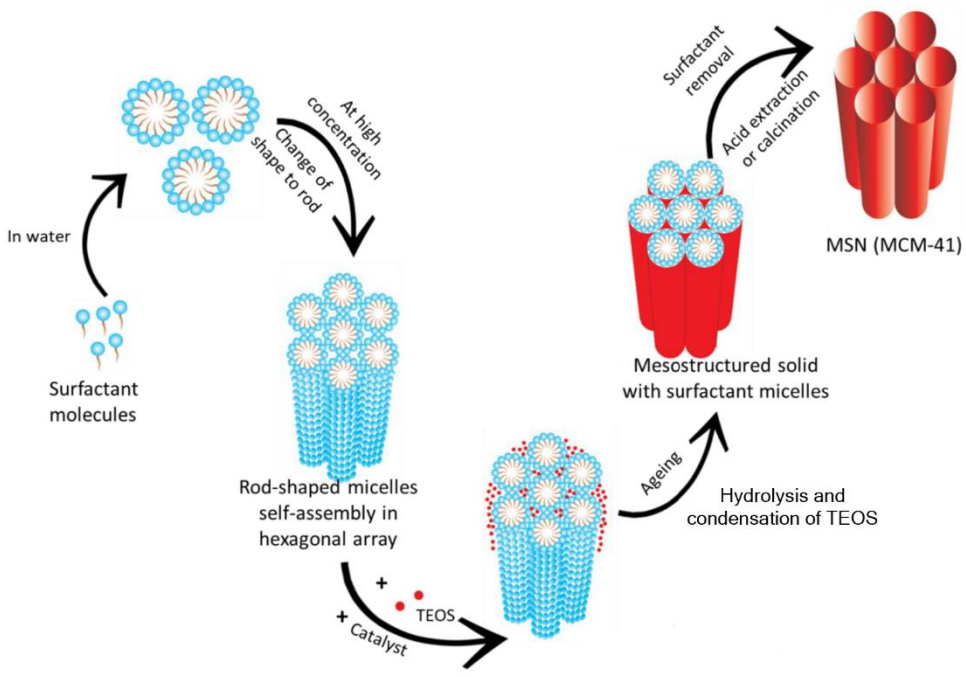

Figure 4 – Synthesis of Mobil Crystalline Materials (MCM). Adapted [17].

In the swelling-shrinking mechanism, represented in Figure 5, tetraethyl orthosilicate (TEOS) is used as the precursor in the absence of any other solvent like ethanol. In water, the cationic surfactant cetyltrimethylammonium bromide (CTAB) forms ellipsoidal micelles with a hydrophobic core where TEOS gets solubilized, thus enlarging the micelles that switches from ellipsoidal to spherical shape. The hydrolyzed monomers of TEOS become hydrophilic leaving the micelles core to the aqueous surroundings. These monomers are negatively charged so they get adsorbed onto positively charged CTAB micelles via electrostatic attraction. During the consumption of TEOS, the micelles become smaller until all TEOS gets hydrolyzed and the silica shell is formed around the micelles through the reaction of condensation of hydrolyzed TEOS. Finally, the micelles aggregate, resulting in particle growth forming a mesoporous structure [33].

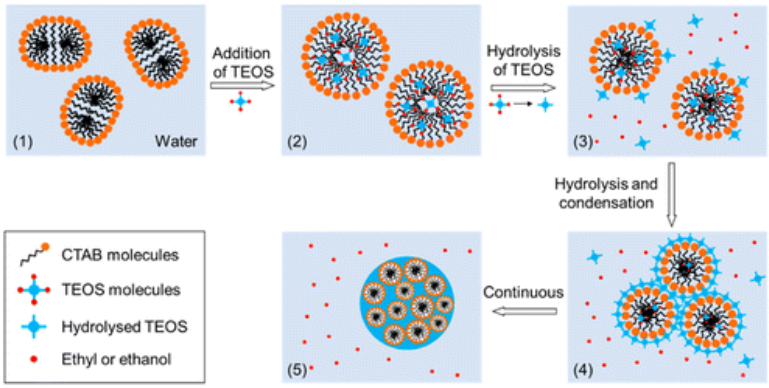

Figure 5 - Swelling-shrinking mechanism [33].

An effective way to control the nanoparticle size is by adding agents like alcohols, amine, inorganic bases and inorganic salts. Such compounds alter the hydrolysis and condensation of the silica precursor, accelerating the reaction kinetics [17]. The reaction parameters equally influence the particle size of MSNs. On increasing the temperature of the reaction, an increase in the particle size was observed [34]. This may be due to the increase in the rate of reaction leading to polycondensation of the silica monomers resulting in a dense silica structure and a larger size. The amount of silica precursor TEOS also influences particle size that was found to increase with an increase in the amount of TEOS. It was also found changes from monodisperse to heterogeneous particle size distribution, which may be attributed to the secondary condensation reactions taking place due to the presence of excess silica precursor which starts producing new nuclei amongst the already existing silica particles [17].

Mesostructural ordering is also influenced by TEOS and CTAB concentration. Higher concentrations of TEOS conduced to disordered mesostructure, however lower concentration may not be enough to form a mesoporous structure. Higher concentrations of CTAB also conduced to disordered structure, however lower concentration led to failure in micelles formation. Cetyltrimethylammonium chloride (CTAC) is known to generate MSNs with the wormhole-like arrangement [17].

Tetra-alkylammonium salts such as CTAB and CTAC are the most widely used family of surfactants used to prepare ordered mesoporous silicas. The type and extent of the hydrophobic groups of these salts determine the pore size of MSMs. For example, pore size can enlarge from 1.6 to 4.2 nm by increasing the surfactant chain length from C8 to C22. Using small-molecule surfactants such as CTAB a pore size less than ~ 5 nm is obtained, such as the pores of MCM-41 [31].

The shape of MSNs is an important parameter once it influences the cellular uptake and biodistribution of the nanocarrier [17]. The morphology of a MSN may be spherical, rod, ellipsoid, film, cube or platelet, each suitable for a specific biological application [31]. MSNs of well-defined shape are internalized by nonspecific cellular uptake and have an influence on cell behavior including protein expression. For example, the long rod-shaped MSNs reduced cell viability/apoptosis severely compared to short rod-shaped and sphere-shaped MSNs. One way to understand such behavior is by considering that NPs of long rod-shaped MSNs are more easily taken up via cell endocytosis than other MSNs [35]. The molar concentration of surfactant, water, base catalyst and TEOS have an impact on the morphology of the MSNs. The transformation in shape of the MSNs may be attributed to the different types of interaction such as hydrogen bonding, hydrophobic interactions between the organoalkoxysilane and the surfactant template. Several ways to control MSNs shape are described in the literature [17]. In order to synthetize sophisticated MSNs a dual-surfactant system may be used, as well as inorganic and organic additives, producing MSNs with specific shapes [31].

A couple of low-cost methodologies have been developed in alternative to the commonly used sol-gel process, including an electrochemistry assisted approach [36], a microwave-assisted method [37] and a sonochemical synthesis [38].

Alternatives to the commercially available substances used in the synthesis of MSNs have been explored, due to high cost and the negative environmental impacts of the reagents

and the harsh synthetic conditions [39]. These alternatives include different natural materials like pumice rock [40], rice husk, and renewable biomass, making scale-up easier, reducing costs and toxicity as well as proffer solutions to the environmental and health threats associated with sustainable biomass waste removal [39].

3.3. Loading and release of molecules from MSNs

The encapsulation of nutraceutical into nanocarriers has emerged as a promising strategy for overcoming pharmacokinetic limitations after oral administration of nutraceuticals. In this context, the co-encapsulation of nutraceutical with a chemotherapeutic agent in a single nanocarrier, has gained wide recognition in recent years because it may generate synergistic effects, enhanced bioavailability and reduce toxicity [1], [41]. An example of this synergy is the capacity of curcumin, a nutraceutical, to increase the sensitivity of some breast cancer cells to multiple chemotherapeutic drugs including cisplatin, doxorubicin and paclitaxel [8]. Combination of the anticancer drug paclitaxel with thymoquinone, a nutraceutical, also demonstrate to have synergetic effects when applied to breasts cancer cells treatment [42]. Another example of combination strategy is the co-delivery of doxorubicin and siRNAs (small interference RNA) using MSNs is into multidrug-resistance cancer cells [43].

MSNs are considered ideal carriers for poorly water-soluble drugs [6], although they are able to encapsulate both hydrophobic and hydrophilic compounds due to their highly available pores [29]. The presence of silanol groups (Si-OH) provides silica hydrophilicity, whereas siloxane groups (Si-O-Si) provide silica surface hydrophobicity. Silanol groups can also provide interaction points with adsorbed molecules, through hydrogen bonds with proton donor/acceptor groups of the hosted molecules. However, these weak interactions are easily broken by water, leading to fast release of adsorbed molecules [31]. Furthermore, owing to surface silanol groups, the surface properties of MSMs can range from hydrophobic to hydrophilic, once silanols render the silica surface hydrophilic and provide interaction points that can be potentially derivatized to yield functional groups that can further increase the interaction strength with incorporated guest molecules, thus providing the possibility of a proper drug loading parameters as well as drug release profile for different drug substances [31]. MSNs are seen as next generation pharmaceutical carriers due to their ability to enhance the efficacy of drugs by improving their aqueous solubility, altering release kinetics,

and targeting via functionalization. Many recent studies have shown that MSNs also improve the aqueous solubility, bioavailability and cell cytotoxicity of hydrophobic drugs [6]**,** and they have been used to demonstrate deliverability of this molecules [29].

One important feature of MSNs influencing biological performance of the encapsulated substance is the surface functionality [29], which influences toxicity, biocompatibility, drug loading and release, biodistribution, and cellular internalization [31]. These nanocarriers can be surface modified with targeting ligands so targeted drug delivery can be achieved, resulting in lower adverse effects [1]. The surface modification may be achieved by covalent conjugation with small functional groups [18]. There are also noncovalent methods and the combination of noncovalent and covalent methods may also be a strategy for surface modification of MSNs [44]. Surface modification of silica particles may be easily achieved by reaction with alkoxysilanes or halosilanes. Alkoxysilanes links to the surface in a condensation reaction with the silanol groups forming 1–3 Si–O–Si. Halosilanes hydrolyze substituting the halide for alcohol group which can also undergo condensation forming 1–3 Si–O–Si links with silanol groups. However, in anhydrous conditions, halosilanes will react directly with surface silanol groups [45]. Surface functionalization of MSNs is not limited to just one ligand, multiple ligands can be anchored [17]. In Figure 6 are represented MSNs covalently functionalized using two different methods, grafting and co-condensation. Grafting is the most widely used functionalization method. It is a post-synthesis method once the surface functionalization is carried out after preparation of the NPs. It consists in the use of an organosilane surface modifier such as $(R'O)_3SiR$, with diverse organic groups R. The functionalization occurs in both surfaces, interior and exterior. Various types of molecules can be covalently attached to the silica wall, from small to macromolecules, such as polymers and lipids. This method allows to retain the mesoporosity, however the distribution of the grafted groups is not uniform. Co-condensation is a simple method with high degree of incorporation and uniform distribution of the organic units. In this method the functionalization is made by adding the silica source mixed with the organosilane to the surfactant template, during the synthesis of the NPs, which leads to the incorporation of the organic groups into the mesopores. Using this method, calcination cannot be used for template removal, once organic groups are destroyed at elevated temperatures, hereupon nanoparticles must be treated by solvent extraction in order to remove surfactant template [31].

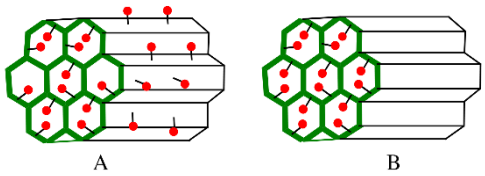

Figure 6 – MSNs functionalized by (A) grafting and (B) co-condensation [31].

Drug loading into MSNs is crucial step and many loading methods are found in the literature including incipient wetness, adsorption by immersion, solvent evaporation, the melt method, co-spray drying, near critical and supercritical CO_2 assisted loading and microwave irradiation [31]. In the incipient wetness method, a known volume of concentrated drug solution is mixed with MSNs to obtain a wet powder in which the drug diffuses into the pores by capillarity. Adsorption by immersion consists in the immersion of the MSNs and a drug solution of concentrations above the adsorption isotherm plateau in an organic solvent, after adsorption, usually after reaching equilibrium state, the loaded silica is recovered by filtration or centrifugation method. In the solvent evaporation method MSNs are dispersed in a drug volatile organic solution and dried by fast solvent evaporation. The melt method according to the physical mixture of drug and silica is heated up until drug melts, can be used only for thermally stable drugs characterized by low viscosity when melted. Adsorption offers the lowest yield and together with incipient wetness, solvent evaporation and spray drying have the inconvenience of using organic solvents. The other three methods offer the control of the amount of loaded drug, but the risk of drug crystallization onto the surface of the silica and of mesopore plugging is major. The melt method can be proposed only for thermally stable drugs with low viscosity when melted. Near critical and supercritical CO_2 as well as microwave irradiation have the advantage of reducing or avoiding the use of organic solvent which then must be removed with potential environmental harm and high costs. These two methods also offer positive results in terms of improvement of drug dissolution, however more investigation is still needed. At the loading step, strong interactions are preferable in order to stabilize the molecule in its amorphous form, whereas at the release step, strong repulsion would be preferred in order to rapidly release the drug from the carrier matrix, which meets the usually loading conditions (non-polar) as well as release conditions (aqueous conditions) [31].

Another important parameter to have into consideration is the controlled release of the substance from the nanocarrier. Controlled and intelligent delivery of drugs to the target site through MSNs is possible due to gated release [17]. In this matter, MSNs can be coated with a biodegradable polymer as a gatekeeping layer [5]. The addition of some functional groups on the surface of mesoporous silica is utilized for inducing specific host-guest interactions with drug molecules. Functionalization with COOH for basic drug molecules and NH_2 for molecules carrying acidic groups, this approach leads to a retarded release rate [31]. Some molecules act like gates of the pores opening only in response to certain stimuli like pH, temperature, chemicals, enzyme, redox, light, ultrasound and so on. Gated drug release is especially effective when drugs presents toxic side effects to other organs [17]. A controlled release system for the gastrointestinal tract (GIT) may be a pH dependent release system, based on the different pH values in different parts of the GIT, varying from pH 1.0 to 3.0 in the stomach, pH 6.5 to 7.0 in the small intestine, and pH 7.0 to 8.0 in the colon. A charged mesoporous silica nanoparticle-based drug delivery system for controlled release and enhanced bioavailability was patented this system may be applied for preparing a colonic drug-sustained-release system [46]. Poly (lactic acid)-coated mesoporous silica nanosphere were used for controlled release of venlafaxine. This material showed good potential in controlled drug-release application, due to pH-sensitive property which tended to decompose quickly in acid media. This NP significantly delay the release of the drug in intestinal condition compared with gastric acid surrounding due to the fast decomposition rate of PLA in gastric acid. The enzyme pepsin, an enzyme from the GIT, played a favorable obstruct role reducing release rate [28].

3.4. Toxicity and biodistribution of MSNs

Most of the reports showed that MSNs get preferentially accumulated in the liver and spleen following administration [17]. It is widely accepted that the uptake of NPs, in oral administration, is through the gastrointestinal epithelium. Penetration in the intestine is greatly dependent on the particle sizes. For example, NPs with the mean size of 50 nm could be absorbed by the gastrointestinal tract, smaller or bigger particles are barely absorbed. Skin is another main entry route for external substances into the body, owing to the large surface area and accessibility to environment. It was discovered that the well-dispersed amorphous nanosilica particles with the average size about 70 nm could break through the skin barrier

and caused systemic biodistribution in mice after repeated topical application exposure, however causing irritation [47]. It was also reported that NPs could be distributed to the same organs by various exposure routes through blood circulation system [48]. Liver was found to be the target organ after intravenous, oral, and hypodermic administration once it is the main organ for removing circulating macromolecules and microorganisms. Excretion of silica NPs may be either through feces or urine [49]. For Mesoporous Hollow Silica NPs (MHSNs) LD_{50}, in mice, $_{was}$ found to be higher than 1000 mg/kg. Mortality, clinical features, pathological examinations, and blood biochemical indexes revealed low *in vivo* toxicity of MHSNs. However, more extensive series and long-term toxicity studies are needed to ensure safety of this materials [50].

4. Nanotechnology in Food Science

Nanotechnology has become an important means of producing novel materials and structures for a wide range of applications within the food industry [2], including some products already available worldwide. For example, nanoparticulate carotenoid lycopene (LycoVit by BASF), a European product that was claimed for use as a food supplement and food fortifying agent. This product has been classified as GRAS by the FDA (BASF US Patent US5968251) [51]. It can be considerate as a promising technology in food science and food industry, once it has been proving its competence and applicability in food systems like processing and packaging [52]. Interestingly NPs can be naturally presented in food and consumed, for example, casein micelles in milk are between 50 and 400nm as the complexes of three subgroups of casein molecules (αs-casein, β-casein, and κ-casein) [21].

Comprehensive descriptions of the manufacture and characteristics of different types of NPs suitable for food applications have been provided by different reviews [2]. According to their composition, NPs used in food packing materials and designed to incorporate foods can be divided into inorganic (metals, metal oxides, etc.) and soft engineered NPs (proteins, polysaccharides, lipids, etc.) [21].

NPs have been employed to address challenges related to food quality, shelf life, cost, safety, and nutritional benefits [21]. They may be applied in packaging, nanoencapsulation, nanosensors, protection against biological deterioration, protection against chemical

ingredients and enhancement of physical properties. Examples of the functionality and applicability as well as safety assessments of nanotechnology in food science are given in Figure 7 [52]. Despite all potential applications of NPs in the food industry and food science the acknowledgment of nanotechnologies in these fields is relatively slow, especially when compared to other applications of nanotechnology like in biomedicine, electronics, catalysis, and energy. The reasons for this may be associated with the public perception of nanotechnology, subsequent labeling and potential regulatory burdens [21].

An example of the applicability of the nanocarriers are the engineered water nanostructures enriched with commonly used sanitizers such as H_2O_2, citric acid, and lysozyme, that came as a promising chemical-free sanitation technology for food safety applications [53]. It was found that mesoporous materials can also be used for food purposes [6],[7].

Similar to what happens in nutraceutical carriers, NPs used for food applications have some important properties such as the chemical composition, size distribution, surface charge, surface area, surface contact, dissolution rate, and bioavailability. The chemical composition and morphology are important factors that determine how NPs interact in the gastrointestinal tract and their subsequent physiological effects that may have an impact on the gut microbiome, and other potential effects to the body [21].

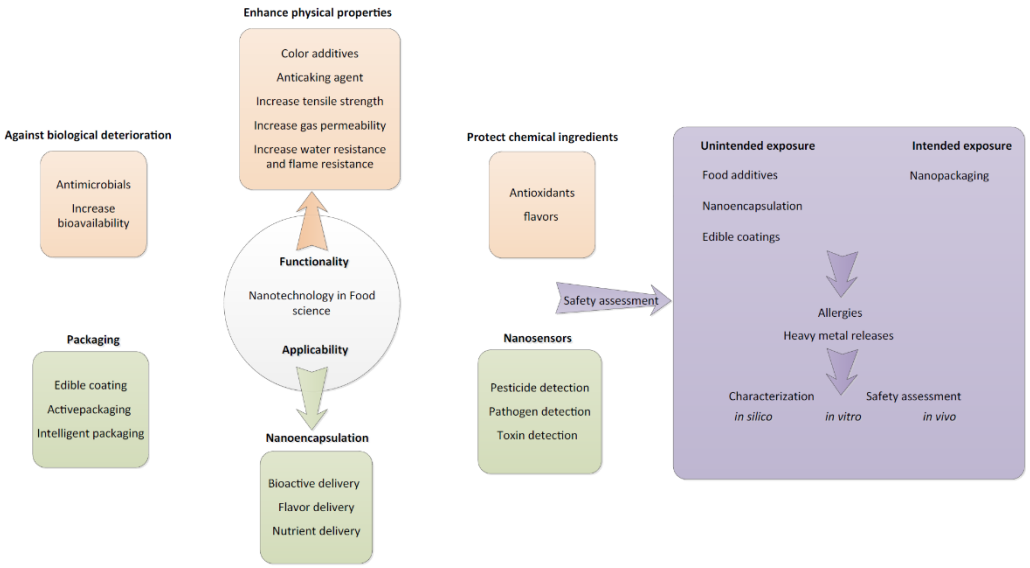

Figure 7 - Diagram of functionality and applicability of nanotechnology in food science/industry [52].

Most of the excipients used in the fabrication of nanocarriers have attained GRAS status by FDA [20] what can be seen as an advantage once it can help to avoid concerns about the toxicity of nanocarriers. However, more studies are needed to evaluate the potential toxicity of the presence of nanomaterials in foods, by analyzing food samples used in food additives/ingredients and food packaging. Little is known about the bioavailability, biodistribution, routes of nanomaterials, and the ultimate toxicity upon exposure to them. The environment impact of these materials is another important matter that has to be taken into consideration [52].

Public perception of nanotechnologies is important for the acceptance of this technology in food and consequently its commercialization. Statements such as "This product contains NPs" or "Manufactured using nanotechnologies" may raise public concerns, especially with sporadic reports about potential adverse effects of certain nanomaterials. Regulation agencies have not yet reached an agreement on worldwide applicable rules. Multiple Agencies and Organizations like the United States Environmental Protection Agency, National Institute for Occupational Safety and Health, the FDA, the Health and Consumer Protection Directorate of the European Commission, the International Organization for Standardization and the Organization for Economic Cooperation and Development, among other regulatory Institutions have been arguing and developing guidance documents with respect to the potential risks posed by nanomaterials [52].

5. MSN-RSV the system as a nutraceutical: Previous works

Several studies have tried to improve RSV physicochemical properties by incorporating it into various nanocarriers including liposomes [56]–[60], cyclodextrins [27], [61], [62], solid lipid NPs [63]–[65], polymeric micelles [66], [67] and polymeric NPs [68]–[71]. However, these formulations suffer from limitations related to poor stability, low drug loading and high production costs. Therefore, it becomes pertinent to develop superior cost-effective delivery nanocarriers for nutraceuticals such as RSV [6]. Taking this into account, in the recent years, has been explored the possibility to use MSNs as nanocarriers for encapsulation and delivery of RSV, some examples are given below.

In 2011, Chih-Hsiang Tsai *et al.* [72] have synthetized mesoporous nanomaterials containing undec-1-en-11-yltetra(ethylene glycol) phosphate monoester surfactant (PMES) inside the pores (PMES-MSNs). This system showed excellent biocompatibility *in vitro*, cellular internalization and endosome escape of PMES–MSNs in cervical cancer cells was demonstrated. The hydrophobic environment created by PMES within the pores improved capacity of PMES–MSNs to be used as drug delivery carriers for RSV. This surfactant-assisted delivery strategy was tested under physiological conditions showing an increase of the drug loading compared to the material without surfactant and steady release of RSV.

MSNs studies go beyond biomedical applications, Valeriu Cotea *et al.* [73], evaluated the ability of SBA-15 to absorb bioactive polyphenols from red wine, including RSV. The studied reveal that SBA-15 has strong retention capacity for cis-RSV and reasonable retention capacity for trans-RSV.

Margarita Popova e*t al.* [74], in 2014, used two different kinds of MSNs, KIL-2 has a disordered mesoporous structure and MCM-41 showing an ordered 2D hexagonal pore arrangement, to load RSV employing two distinct preparation methods: loading by mixing the RSV with the mesoporous carrier in solid state and impregnation by contact with an ethanolic solution of RSV. They found that these silica supports are suitable for stabilization of *trans*-RSV and reveal controlled release and ability to protect the supported compound against degradation regardless of loading method. The solid-state dry mixing appears very effective for preparation of drug formulations composed of poorly soluble compounds.

Rongrong Zhang *et al.* [75], in 2015, prepare and evaluate RSV-loaded MSNs modified by amino groups, in order to improve the bioavailability of RSV. Samples were synthesized by modified Stober method and loaded using a repeated saturated solution adsorbing method, resulting in a large amount of RSV encapsulated. Transport ability and pharmacokinetics were studied., resulting in a release quantity of 73.3% in 48h, transmembrane transport was much larger than in free RSV.

N. Summerlin *et al.* [6], in 2016, claimed to be first reporting a successful encapsulation of RSV within MSNs with high drug loading and enhanced biological activities, however, as cited above previous works in this field were find in the literature. MCM-48-RSV was the denomination given to the system of colloidal mesoporous silica NPs loaded with RSV. The saturated solubility, drug release, anti-inflammatory and anticancer

efficacy against colon cancer cells, of the system were studied. MCM-48-RSV presents increased *in vitro* release kinetics compared to pure RSV, shows high loading capacity (20% w/w) and excellent encapsulation efficiency (100%) enhancing saturated solubility of RSV about 95%. MCM-48-RSV-mediated *in vitro* cell death (HT-29 and LS147T colon cancer cell lines) was higher than that of pure RSV. The anti-inflammatory activity improvement was also demonstrated, once MCM-48-RSV treatment inhibited lipopolysaccharide-induced NF-κB activation in RAW264.7 cells. For these reasons this study proposes colloidal MSNs as next generation delivery carriers for hydrophobic nutraceuticals.

Estelle Juère *et al.* [76] observed that the permeability of RSV encapsulated in MCM-48 NPs can be enhanced compared to a RSV suspension when tested through the human colon carcinoma cell monolayer (Caco-2). They demonstrated that RSV encapsulation did not alter its bioactivity and, at lower concentration of MCM-48 containing RSV ([MCM-48-RSV] = 5 μg mL^{-1}), RSV encapsulation provided higher anti-inflammatory activity compared to both RSV suspension and solution, it was also observed that the saturated solubility could depend not only on the pore size but also on the particle size of the nanocarriers. This study also supports the potential of MSNs as next generation nanocarriers for hydrophobic drugs and nutraceuticals.

Yang Shen *et al.* [5] were able to load RSV into polylactic acid (PLA)-coated MSNs. PLA coating works as a gatekeeper preventing RSV from burst release, while reactive oxygen species (ROS) triggers the drug release by accelerating PLA degradation. *In vitro* studies with a co-culture of rat brain microvascular endothelial cells (RBECs) and microglia cells used as a blood–brain barrier (BBB) was established to evaluate RSV delivery across BBB. These carriers were conjugated with a ligand peptide of low-density lipoprotein receptor (LDLR) that markedly enhanced the migration of MSNPs across the RBECs monolayer. This study conclude that RSV could be released and effectively reduce the activation of the microglia cells stimulated by phorbol-myristate-acetate or lipopolysaccharide.

Zanib Chaudhary *et al.* [29] successfully encapsulated RSV within negatively and positively charged MSNs with phosphonate (PO_3-MSNs) and amine (NH_2-MSNs) groups respectively. At pH 7.4 both free and loaded NH_2-MSNs RSV showed burst release with almost 90% of drug released in first 12 h, PO_3-MSNs showed only 50% drug release in the

same period. At pH 5.5, both the PO_3-MSNs and NH_2-MSNs showed significant control over release, around 40% less release compared with free RSV in 24 h. PO_3-MSNs significantly enhanced the anti-proliferative potential of RSV on the other hand NH_2-MSNs didn't affect proliferation.

In order to improve therapeutic efficacy against gastric carcinoma, Hu Yu *et al.* [77], developed (anti-miR21 and RSV)-loaded MSNs conjugated with hyaluronic acid, which works as a targeting ligand. This study confirmed the enhanced anticancer effect showing significant reductions in the tumor burden with a 3-fold higher tumor regression effect when compared to free RSV.

The previously presented studies provide insights of the applicability of MSNs loaded with polyphenols such as RSV in human health and disease treatment, including is potential as next generation anticancer formulations.

6. Purpose of the study

The aim of this work is to prepare nutraceuticals based in mesoporous silica nanoconjugates with RSV. To achieve this main goal the first step is to synthetize MSNs, as described in section II. Materials and Methods, followed by a proper characterization of the obtained nanomaterials using various methodologies, are they FTIR, BET, Zeta potential, DLS, STEM and XRD which results are presented in sub-section 1 Characterization of section III Results and Discussion. The procedure for the synthesis of the MSNs was based on methodologies described in the literature [78]. Different synthesis conditions were tested in order to evaluate the effects of the reaction parameters on the obtain materials and so optimize the synthesis procedure. The loading capacity of the synthetized MSNs for RSV was tested using to different procedures, sub-section 2 Loading of RSV (III. Results and Discussion) comprise the comparation between the two techniques of loading, the loading capacity and characterization of the loaded material. The release kinetics, of loaded materials, in two different pH values, 7.4 as the physiological pH and 5.2 mimicking the acidic environment of some tumorous tissues, are described in sub-section 3 In vitro release studies.

Because of time issues and other unpredictable situations, it was not possible to achieve all goals drawn for this work. Testing the RSV-MSNs systems in melanoma cells was one of the main goals, and as not been reported yet, however by the time of ending this work test were still ongoing.

II. Materials and Methods

Applied chemicals

Hexadecyltrimethylammonium bromide (CTAB, 99.0%), tetraethyl orthosilicate (TEOS, 99%), phosphate buffered saline pH 7.4 (0.01 M PBS, 25 ºC) packets and the dialysis cellulose tubing membrane (3 kDa cut off) were purchased from Sigma-Aldrich. Triethanolamine (TEA, 99%) and sodium chloride (NaCl, 99.5%) were obtained from Fisher Chemical. Trans-RSV (99%) was purchased to Tokyo Chemical Industry. Methanol and ethanol absolute from VWR. Dionized (Mili-Q®) water was used in all experiments. All chemicals were used as received without further purification.

Synthesis of the MSNs

The MSNs were prepared by a simple method adapted from literature [78] and based on (an aqueous) biphasic system. Briefly, 2,0 g of surfactant (CTAB) were dissolved in 20 mL of Milli-Q® water. The solution was then moved to a round bottom flask immersed in an oil bath under constant stirring (450 rpm). Then, after the solution reached 95 °C, 50 or 100 µL of TEA was added and the resulting solution was stirred for one hour. Afterward, 1,5 mL of TEOS was add drop wise and the reaction was left to occur for 1, 6 and 24h. Temperature was controlled during all synthesis process, and the reaction occurred in reflux conditions to ensure the maintenance of concentrations (Figure 8).

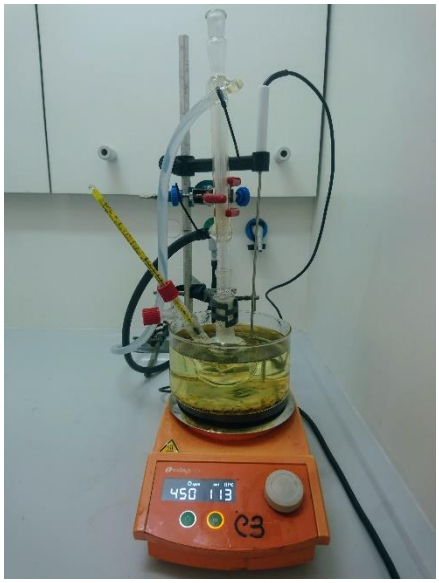

Figure 8 – Synthesis apparatus photograph.

The MSNs were collected by centrifugation (13 300 rpm for 10 minutes) and washed three times with ethanol to remove the residual reactants. To remove the surfactant (and facilitate the calcination process) all the collected products were extracted for 4 h with a 1wt% solution of sodium chloride (NaCl) in methanol at room temperature to remove the (CTAB) template. One last wash with ethanol was made, with the same conditions as the ones made after the synthesis, so NaCl could be washed out. Finally, for complete removal of surfactant, MSNs were calcinated in a muffle furnace (Termolab) for 10h at 550 °C. The samples were obtained labelled as nBX.Y, where n=sample number, X=1, 6 and 24 (reaction time after TEOS addition), and Y= 50 or 100 (volume of TEA) -Table 1.

Table 1- Scheme of the synthesis with reaction conditons for each sample.

Sample	Nº of the sample	Reaction time (h)	Quantity of TEA (µL)
1B1.50	1	1	50
2B1.50	2		
3B1.100	3		100
4B1.100	4		
5B6.50	5	6	50
6B6.50	6		
7B6.100	7		100
8B6.100	8		

9B24.50	9	24	50
10B24.50	10		
11B24.100	11		100
12B24.100	12		

Physicochemical characterization

Fourier-transform infrared (FTIR) spectra were collected on a Mattson–7000 spectrometer, using KBr technique. 256 scans were collected per sample over the range of 4000 to 300 cm^{-1} at a resolution of 2.0 cm^{-1}. Nitrogen adsorption−desorption isotherms at 77 K were measured on a Micrometrics Gemini V2.0 (Micromeritics Instrument Corp.) system. All samples were pre-treated for 5h at 473 K under nitrogen before measurements. The pore size was calculated from desorption branches of isotherms by the Barrrett-Joyner-Halenda (BJH) method. Surface areas were calculated by the Brunauer-Emmett-Teller (BET). Zeta potential measurements and dynamic light scattering analysis were performed in a Zeta Sizer Nano Plus equipment (Malvern Instruments). Zeta potential measurements were performed by suspending the MSNs in Milli-Q® water at different pH values (2, 4, 6, 8 and 10). Equilibration time established was 120s (for each sample) and 3 measurements were performed with 100 runs each. For DLS measurements the NPs were suspended in PBS buffer (pH 7.4) and dispersed in an ultrasound bath for 5 minutes. Equilibration time was 120s and 3 measurements were performed with 11 runs of 10s each. Size and morphology of MSNs were investigated by scanning and transmission electronic microscopy (STEM) using a Hitachi H-9000 equipment, operating at 300 kV. Samples were prepared by evaporating dilute suspensions of the NPs in ethanol on a copper grid coated with an amorphous carbon film. Powder X-ray diffractograms were recorded using a PANalytical Empyrean diffractometer Kα(Cu) radiation with a curved graphite monochromator (step 0.05º) in the range $10º < 2\theta < 65º$. Thermogravimetric analysis (TGA) was employed to access the amount of RSV loaded on the MSNs, in a Hitachi STA300 equipment with a heating rate of 5 ºC/min (temperature range 30-800 ºC), under a nitrogen:oxigen atmosphere (3:1). Elemental analysis (C and H) was performed on a Truspec 630-200-200 equipment. Heating curves of MSNs were obtained using differential scanning calorimeter (DSC) in a Perkin Elmer, Diamond DSC. Samples were weighed and loaded into a hermetically crimped

aluminium pan and heated under a nitrogen purge at the rate 50 mL/min, from 30 to 350°C at the heating rate 10°C/min. UV-VIS spectra were obtained in a GBC Cintra 303 spectrophotometer operating in the range 200–500 nm.

Preparation of RSV loaded MSNs

Two distinct loading methods were tested for loading RSV into the MSNs, the rotary evaporation and the immersion technique.

Rotary evaporation technique

RSV loading was performed using the rotary evaporation technique [6], [29], [76]. In a typical procedure 40 or 80 mg of RSV were dissolved in 10 mL of ethanol and the solution was placed in an ultrasonic bath for 4 min. Afterwards, 100 mg of the NPs were added to the solution and the dispersion was placed in the ultrasonic bath for 10 min. The solvent was then evaporated at 50 °C in a rotary evaporator until all ethanol was removed, to obtain the RSV-loaded MSNs (RSVEV, 7.40 and 7.80). The final solids were scratched off from round bottom flask and stored at room temperature, protected from light with aluminum foil.

Immersion technique

The procedure was identical to the one used in the rotary evaporation method however after suspending MSNs in the RSV solution, the suspension was stirred at room temperature for 65h protected from light. The final solids were collected by centrifugation (13 300 rpm for 10 minutes) and stored protected from light with aluminum foil.

***In vitro* release studies**

The *in vitro* release studies were performed in PBS at two different pH values, pH 7.4 and 5.2. The suspensions were prepared by dispersing the RSV-loaded MSNs (equivalent to 500 μg of free RSV) in 1 mL of PBS, introduced into a dialysis membrane (with a 3.5 kDa molecular weight cut-off) and immediately immersed in 29 mL of PBS. The

experiments were kept under continuous but gentle stirring at 37 °C, protected from light. At predetermined time intervals 1 mL of the sample was withdrawn and immediately replaced with an equal volume of PBS to maintain sink conditions. For comparison, the test was also performed using free RSV. The removed samples were analyzed for RSV content using UV-VIS spectroscopy (r^2 = 0.99996 and r^2 = 0.9992 for pH 7.4 and 5.2, respectively), at 305 nm (Figure 1sa, Figure 2sa and Figure 4sa, Supplementary material). The cumulative release percentage of RSV was calculated using Equation 2:

$$Cumulative\ release\ (\%) = \frac{Volume\ of\ sample\ withdrawn\ (mL)}{Bath\ volume\ (mL)}\ X\ P(t-1) + Pt \qquad (2)$$

where Pt corresponds to the percentage released at time t and P(t – 1) the percentage released previous to time t.

III. Results and Discussion

1. Characterization

1.1 FTIR

The cationic surfactants CTAB was used as mesoporous templates for synthesis of MSNs and removed through calcination. FTIR analysis was carried out to confirm the complete removal of CTAB, as well as to confirm the presence of the characteristic peaks of silica compounds in the region of 400-1800 cm^{-1}.

FTIR measurements (Figure 9) showed that the surfactant CTAB was completely removed of the calcinated MSNs, according to the absence of the two characteristic peaks in the region 3200–2800 cm^{-1}, which correspond to the asymmetric (2946 cm^{-1}) and symmetric (2877 cm^{-1}) stretching vibrations of the methylene chains. These peaks were present in the non-calcinated MSNs but absent in the calcinated MSNs, which indicates the complete removal of surfactants [79].

All synthesized MSNs showed the characteristic peaks of silica compounds. Analysing the FTIR spectra of synthesized MSNs, the band at 1619 cm^{-1} was attributed to water molecules retained by siliceous materials, 1076 cm^{-1} to Si-O-Si asymmetric stretching, 954 cm^{-1} to external Si-OH groups, 808 cm^{-1} to Si-O-Si symmetric stretching and 455 cm^{-1} to Si-O-Si bending [80].

Bands near to 2300 cm^{-1} were associated with the asymmetric stretching vibration of gas-phase CO_2 that originates from ambient air absorption in the optical path outside the FTIR cell [80].

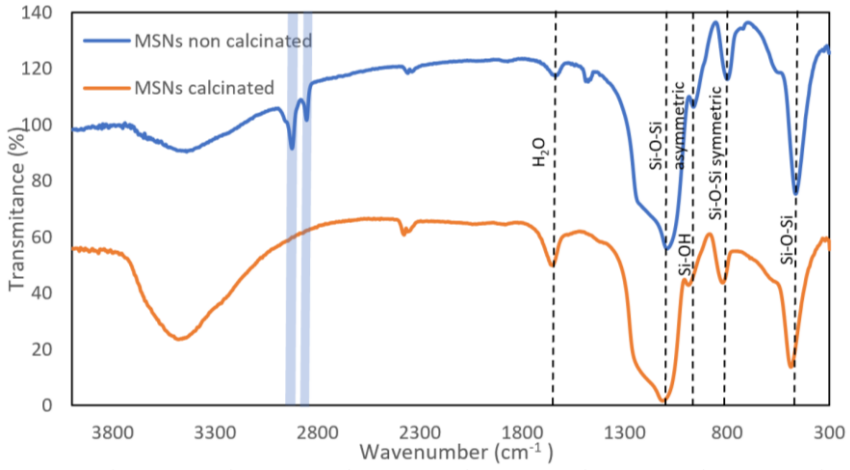

Figure 9 - FT-IR spectra of MSNs before and after the removal of surfactant.

1.2 BET

The textural properties of materials prepared were analysed by N_2 adsorption-desorption technique and the resulting isotherms are shown in Figure 10. According to the IUPAC nomenclature the isotherms could be classified as type IV isotherm with a hysteresis loop [81], [82]. This adsorption behaviour is characteristic of mesoporous adsorbents determined by the adsorbent-adsorbate interactions and by the interactions between the molecules in the condensed state. The first stages, the initial knee of the isotherm, corresponds to the complementation of the monolayer coverage, ending at the called Point B where the middle almost linear section begins in consequence of multilayer adsorption. The initial monolayer-multilayer adsorption on the mesopore walls, is followed by pore condensation, in which the gas condenses to a liquid-like phase. In this case, a type IVa isotherm, the capillary condensation is accompanied by hysteresis, this phenomenon occurs when the pore width exceeds a certain width, which is dependent on the adsorption system and temperature [83]. Only two isotherms are presented in Figure 10, however all samples were analysed, and results were concordant (One other isotherm is showed in Figure 3sa, Supplementary material)

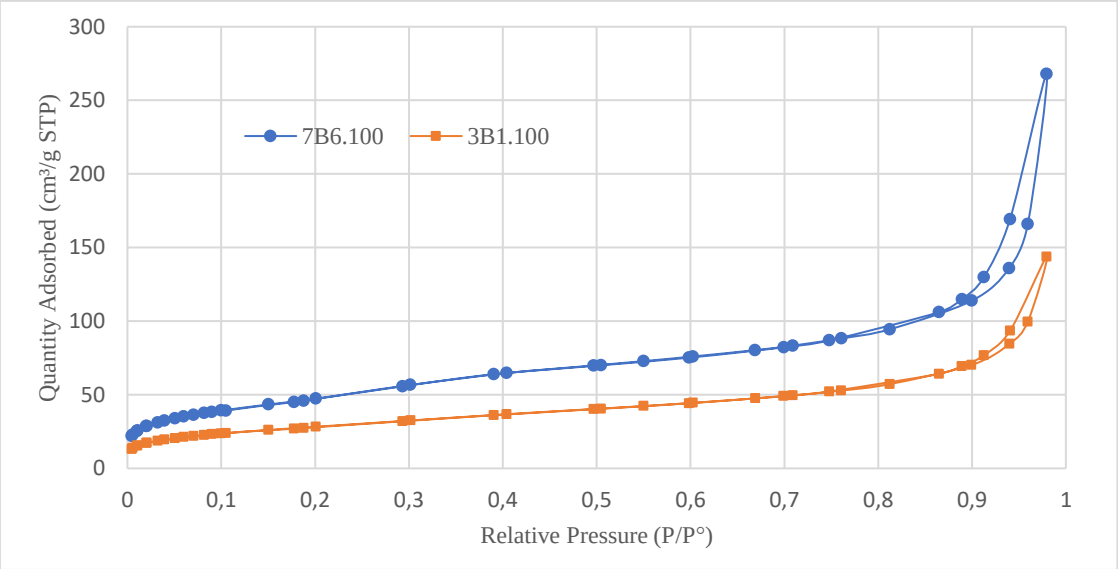

Figure 10 - N_2 adsorption–desorption isotherms of the mesoporous materials after calcination.

Hysteresis is usually associated with capillary condensation in mesopore structures [81]. The isotherms of the samples 3B1.100 and 7B6.100 present hysteresis loop at a high relative pressure, above 0.8. This behaviour is often found in other reported mesoporous materials, and may be attributed to inter-particle porosity [82], [84], [85]. Classifying a hysteresis loop may be a challenging chore, doubts may be raised regarding the profile of hysteresis once characteristics of H1 and H3 loops may be identified. H3 hysteresis loops does not exhibit a limiting adsorption at high relative pressure, these type of loops may be associated with non-rigid aggregates of plate-like particles giving rise to slit-shape pores [81], [86], but also if macropores are present in the pore network, which are not completely filled with pore condensate, [81] presence of macropores may also be suggested by the not horizontal isotherms near p/p°=1. H1 hysteresis loops are characterized by a narrow loop that is indicative of a delayed condensation on the adsorption branch, adsorption and desorption branches are parallel, and a plateau for higher relative pressures. [83] This type of hysteresis is often associated with porous materials known to consist of agglomerates or compacts of approximately uniform spheres in fairly regular array, [81] a narrow distribution of uniform mesopores and limited networking effects [87]. Taking into account the STEM results further discuss in this chapter, these materials are spheres with approximately uniform mesopores, characteristics that are described by H1 hysteresis.

Isotherm quality can be evaluated analysing some features that may be considered suspect. The crossing of the desorption and adsorption branches and the hysteresis extending below relative pressure of ca. 0.38 are typically associated with instrumentation issue or incorrect analysis parameters. Prolonged low-pressure hysteresis, non-closure, is typically associated with experimental artefacts or leaks, however low pressure hysteresis may also be associated with flexibility of the adsorbent structure [83]. Any of these phenomena were observed in the discussed samples.

The textural parameters presented in Table 2 are calculated from the adsorption branch of the respective sample. For Type IVa isotherms the BET (Brunauer-Emmet-Teller) area can be regarded as true probe accessible specific surface area [87]. The total pore volumes were calculated by BJH (Barrett, Joyner and Halenda) method. The average pore size was calculated using the ratio (4*Volume/Area) that considers pores with cylindrical shape.

Table 2 – Textural properties of MSNs after calcination.

Sample	BET Surface Area (m^2/g)	Pore Volume (cm^3/g)	Average Pore Size (nm)
1B1.50	85.3	0.220	9.71
2B1.50	147.2	0.459	10.9
3B1.100	100.9	0.238	8.9
4B1.100	103.6	0.189	6.8
5B6.50	97.2	0.208	8.2
6B6.50	98.2	0.252	9.0
7B6.100	166.6	0.444	9.4
8B6.100	128.5	0.195	5.2
9B24.50	80.3	0.215	10.1
10B24.50	94.8	0.213	8.5
11B24.100	84.1	0.310	14.2
12B24.100	110.6	0.259	8.99

In order to evaluate the effect of synthesis parameters such as time and TEA quantity, in the textural properties of MSNs, N_2 adsorption-desorption analysis was made. The general

tendency is to have an increase of surface area, pore volume and average pore size with the increment of TEA added during the synthesis. This is clearly observed in samples 5B6.50 and 6B6.50, in which 50 µL of TEA was used, relatively with samples 7B6.100 and 8B6.100, made under the same conditions except for the quantity of TEA which in this case was 100 µL. For samples synthesized during 24h, there is an increase in surface area however it is not very significant. Pore volume and average pore size a slightly increase. An exception to this phenomenon occurs between samples 3B1.100 and 4B1.100 relatively to 2B1.50, in this case the samples prepared with higher quantity of TEA presents lower BET surface area, pore volume and average pore size. This influence of TEA on the properties of MSN had already been reported in by Limin Pan *et al.* [78].

The overall impression for synthesis during 24h is that it is not much advantageous, exhibiting similar results as the 1h reaction time. Reaction time of 6h seems to be the one giving the better textural properties.

In all samples, the average pore diameter was larger than 2 nm, which indicates mesoporosity. [29] The tendency found in the literature suggests that typically these materials present higher BET surface area and pore volume, and smaller pore size while this last parameter may vary significantly in different publications, some of them comparable to the presented results [29], [79], [82], [84], [86], [88], [89].

For the same conditions samples tend to have similar textural properties for example 5B6.50 and 6B6.50, synthesized under the same conditions but in different days, have similar surface area, 97.2 and 98.2 m^2/g respectively, and also pore volume and size. However, some exceptions occurred especially in pore volume which revealed to be the parameter with the most variability.

Considering the type of isotherms and hysteresis, and an average pore diameter larger than 2 nm in all samples, it is reasonable to state that the analysed samples are mesoporous materials.

Since sample 7B6.100 showed the best results at BET analysis, it was chosen to proceed with the loading and further drug dissolution studies.

1.3 Zeta Potential

Surface charge and particle size are two commonly mentioned factors that are responsible for a range of biological effects of NPs including cellular uptake, toxicity and dissolution. Studies suggest the influence of these factor in release profile from NPs designed for drug delivery and release at target sites [90].

Zeta potential was measured for three samples, suspending the materials in Milli-Q® water at various pH values from 2 to 10, results are presented in Figure 11. For all pH values the three samples exhibit negative charge values. The negative charges are probably due to the deprotonated silanol groups distribute on silica surface. [91] For pH near 2 zeta potential gets closer to neutral values, behaviour that is typical of silicic acids and can be explained by the weakly acidic silanol groups of the silica surface. [92] The higher the pH the lower the zeta potential is, with exception for pH around 8 in 11B24.100 and 7B6.100 which slightly increases relatively to pH 6. Ich phenomenon does not happen in sample 3B1.100 in which zeta potential suffers a small decrease.

These results may suggest a not significant loss of silanol groups due to heat treatment, once the samples were calcined for 10h, and temperature is known to decrease concentration of silanol groups [93]. Obtained results are in agreement with the ones found in the literature for similar materials, exhibiting an overall decrease of the zeta potential when approaching alkaline conditions and zeta potential near neutral values for lower pH [91], [92], [94].

The magnitude of the zeta potential provides information about particle stability. Particles with high magnitude potentials exhibits increased electrostatic repulsion and therefore increased stability, [95] due to electrostatic repulsion between particles with the same electric charge that cause segregation of the particles [96]. Suspensions with zeta potential out of the rage +30 mV to -30 mV are considered as stable, [97] which means that for these samples it is possible to obtain stable suspensions with pH above 3 for 3B1.100, 3.5 for 7B6.100 and 4.5 for 11B24.100. In all analysed samples suspensions are stable at physiological pH and pH 5.2, this is an important conclusion once suspensions with these pH values were prepared for the release studies.

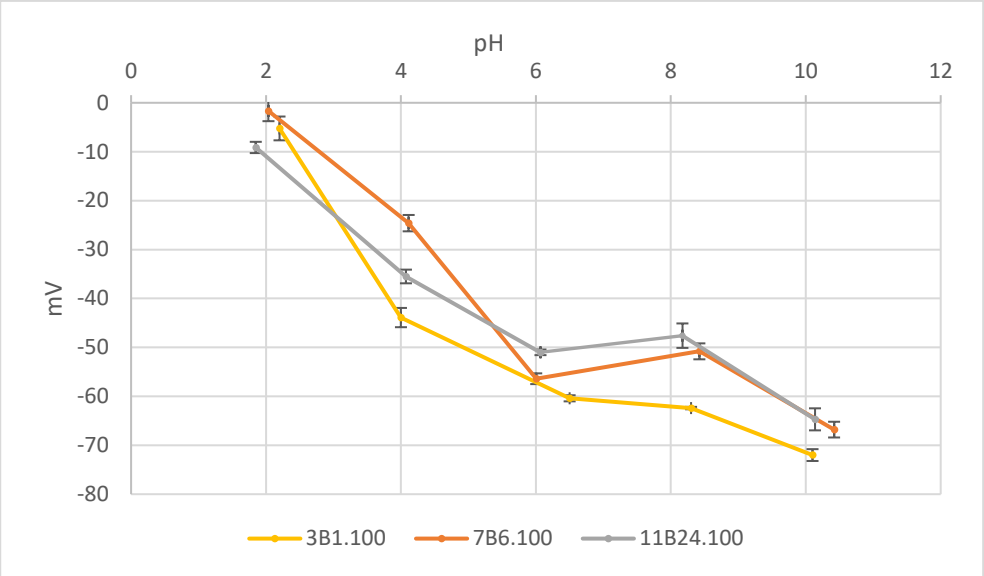

Figure 11 – Variation along pH scale of the zeta potential of 3 samples.

1.4 DLS

Dynamic light scattering measurements are shown in Figure 12. Figure 12 (a) refers to a suspension of NPs in PBS (pH 7.4) while (b) is the same suspension after 5 min of ultrasonic treatment. The first peak of Figure 12 (b) corresponds to a hydrodynamic diameter of 132.5 nm with a standard deviation of 67.47 nm (peak volume of 91.4%). The second peak reveals a hydrodynamic diameter of 4847 nm with a standard deviation of 967.3 nm (peak volume of 8.6%), corresponding to agglomerated NPs. NPs showed a tendency to aggregate and ultrasonic treatment might not be enough for the complete and uniform suspension of the NPs.

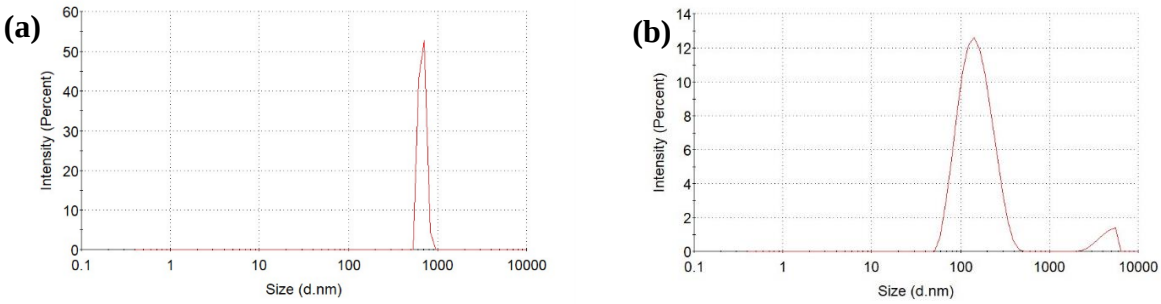

Figure 12 – DLS of MSNs (a) suspended in PBS and (b) after ultrasonic treatment.

1.5 STEM and XRD

STEM technique allowed to observe and determine some important features. NPs showed spherical shape and a visible porous texture as it is clearly seen in Figure 13 (c), this TEM image also suggest a wormhole arrangement as expected for an MCM-41 material, this textural property is also suggested by the XRD diffractograms.

Images showed well dispersed NPs which make possible the calculation of the mean particles size of the analysed samples. For this measurements Image J software was used and results are presented in the histograms of Figure 13 with the respective normal distribution. Mean particle size of sample 7B6.100 was 46 ± 7 nm and 69 ± 5 nm for sample 8B6.100. Both samples were synthesized under the same conditions, however difference in mean particle size is above 30%. Synthesis reaction is very sensitive to changes in conditions, even though synthesis conditions were the same some variables are difficult to control, such as drop rate of TEOS or temperature control after adding TEA or TEOS. Such variables may have affected the properties the synthesized NPs.

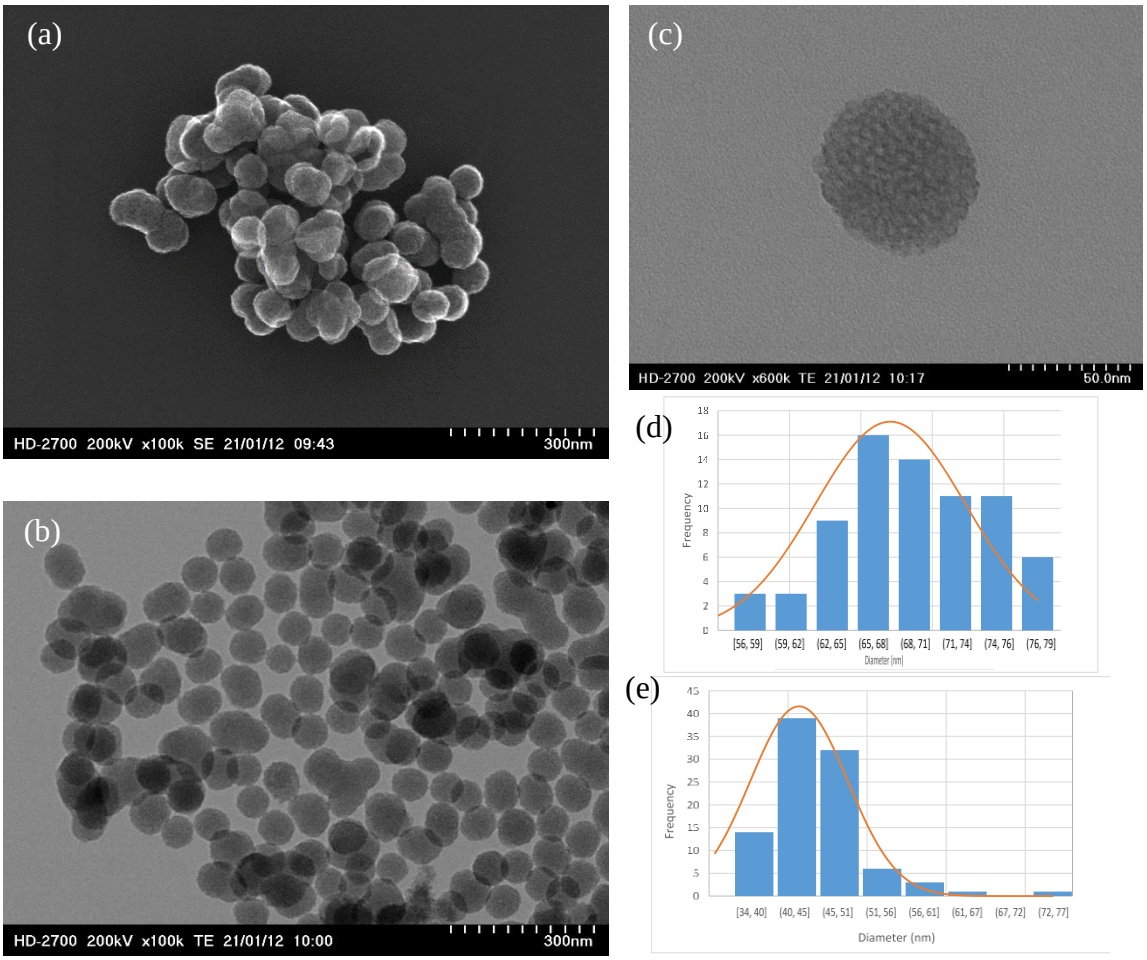

Figure 13 - (a) SEM image of sample 8B6.100; (b) and (c) TEM images of sample 8B6.100; (d) distribution of particle size of sample 8B6.100; (e) distribution of particle size of sample 7B6.100.

The low angle diffractogram from Figure 14 shows a strong broad peak centred at 1.6°, which is outside of the typical range for ordered MCM-41 bulk materials that is usually between 2.2 and 2.5° 2θ for the (100) reflection and two to three more peaks resulting from additional Bragg reflections [98]. Presence of only one broad peak is so indicative of a less ordered material [99]. Results indicate the presence of a material with a mesostructure [100]. Shift towards smaller angles is commonly attributed to deviations in packing of the pores with respect to ordered MCM. Broadening of the peak may be associated with wormhole arrangement of the pore network, although the peak broadening is also expected to happen in small size nanoscale particles [98].

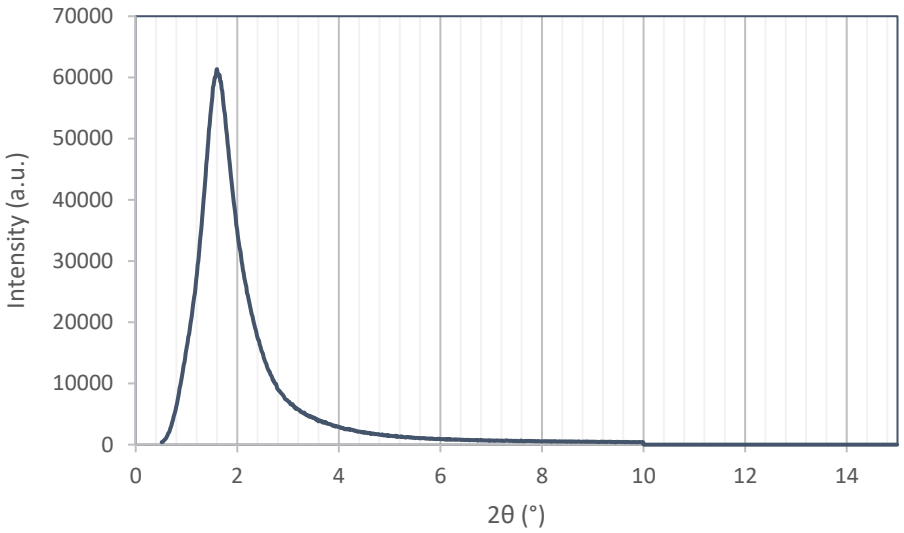

Figure 14 - Transmission XRD pattern of MSNs.

2. Loading of RSV

The MSNs loaded with RSV were prepared following the procedures described in II. Materials and Methods. In a first stage of the work, two different loading methods were used, the immersion method and the evaporation method. The attempts of loading were made with sample 3B1.100. In order to understand which method is the most adequate the following studies were made.

2.1 Comparison of immersion and evaporation loading methods

A sample of MSNs (3B1.100) was loaded with RSV using the immersion method (sample RSV65) and the rotary evaporation methods (sample RSVEV). In both methods the initial amount of RES available for loading was 40 mg.

With the aim of evaluating the presence of RSV in the loaded samples, FTIR spectra of the obtained material were acquired (Figure 15). Differences are clearly seen in the spectra of the NPs loaded in the rotary evaporator when compared to the unloaded NPs, through the appearance of various new bands. Bands from 1587 to 1445 cm^{-1} that can be ascribed to

benzene skeleton vibrations, 987 and 966 cm^{-1} ascribed to bending vibrations of C=C-H [101]. These results indicate that RSV was successfully loaded into the MSNs using the rotary evaporation method. In the spectrum of RSV65 these bands were not visible, and the spectrum was rather identical to the spectrum of the unloaded MSNs.

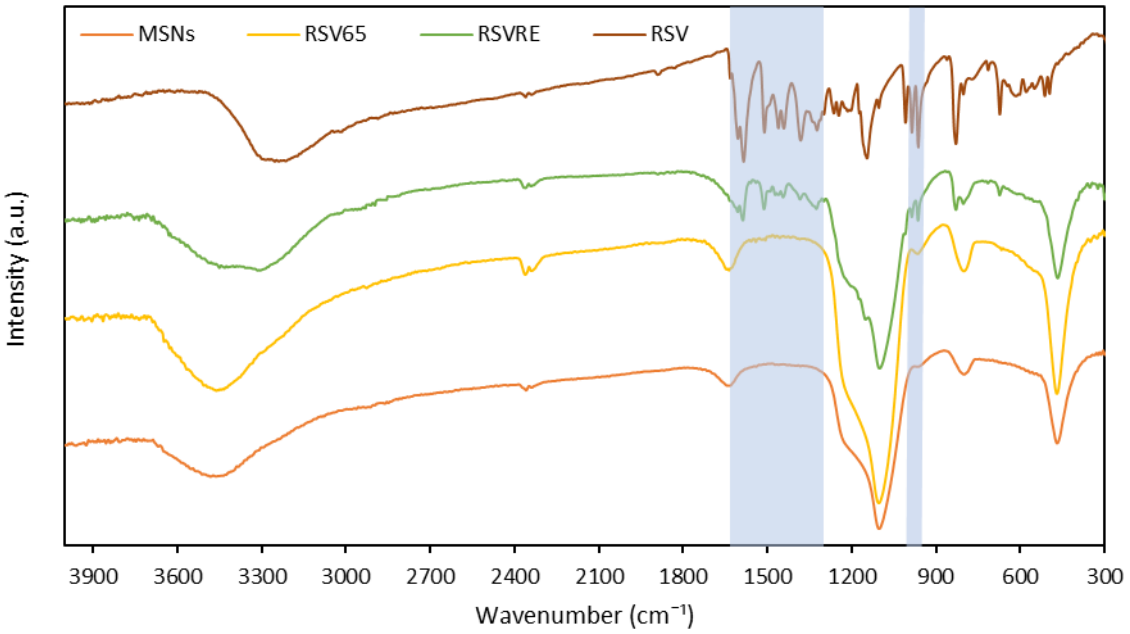

Figure 15 – Comparison of IR spectra of calcinated nanoparticles and loaded using the two loading methods.

The RSV loading capacity was evaluated by TGA analysis. Figure 16 shows the curves of weight loss (%) versus temperature (ºC) for unloaded MSN (3B1.100), pure RSV and MSN loaded with RSV using the evaporation (RSVEV) and the immersion (RSV65) methods.

It is clearly observed that the weight loss of unloaded MSNs is very small. At 700ºC the weight loss was 6.8%, and the curve almost stabilizes for temperatures above 100ºC. The weight loss below 100ºC is probably due to the evaporation of adsorbed water molecules. In the case of RSV, the mass loss occurs in two steps. The weight remains stable until approximately 240ºC and suffers two sharp decreases, followed by weight stabilization above 550ºC with a total weight loss of 99.3%. First decrease may be attributed to the beginning of the thermal decomposition of the material, the second attributed to the oxidation of the carbonized material [102].

The curve of the loaded sample suggests the success of the loading method, which in this case was the one using the rotary evaporator. The profile of this curve is different from the non-loaded MSNs and pure RSV curves.

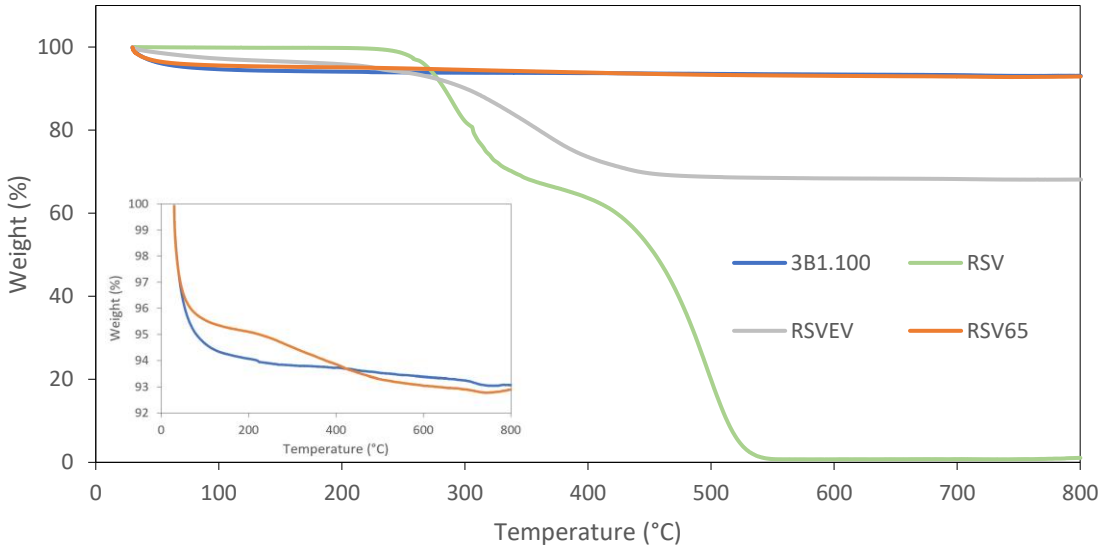

Figure 16 – Thermogravimetric analysis of MSNs (3B1.100), pure RSV and MSN loaded with RSV using the rotary evaporation and immersion methods.

Regarding the loading method of immersion, the TGA curve is also shown in Figure 16. In this case the profile of both samples, loaded and non-loaded MSNs, is very similar. Total weight loss for 3B1.100 was 7.0% at 800ºC and 7.1% for RSV65. Considering that RSV weight is stable until 240 ºC and NPs almost stabilize above 100 ºC, any weight loss was attributed to RSV under 200 ºC. Above 200 ºC weight loss of calcinated NPs was 0.9% and 1.9% for RSV65, indicating that a small amount of RSV was loaded.

The textural properties of two loaded MSNs were also determined through N_2 sorption-desorption isotherms, that are shown in Figure 17. The results suggests the successful loading of RSV onto the MSNs with the rotary evaporator, once the BET specific surface area, pore volume and average pore size decrease (Table 3), which can be explained by the occupation of the mesopores by RSV molecules [29], [84]. On the other hand, data from MSNs immersed during 65h in an RSV solution, suggest the failure of this method once it is observed an increase in surface area, pore volume and pore size, when compared with unloaded NPs (3B1.100).

Table 3 - Textural properties of the MSNs before and after loading using the immersion and evaporation methods.

Sample	BET Surface Area (m^2/g)	Pore Volume (cm^3/g)	Average Pore Size (nm)
3B1.100	100.9	0.238	8.9
RSVEV	40.4	0.070	6.0
RSV65	115.2	0.358	11.7

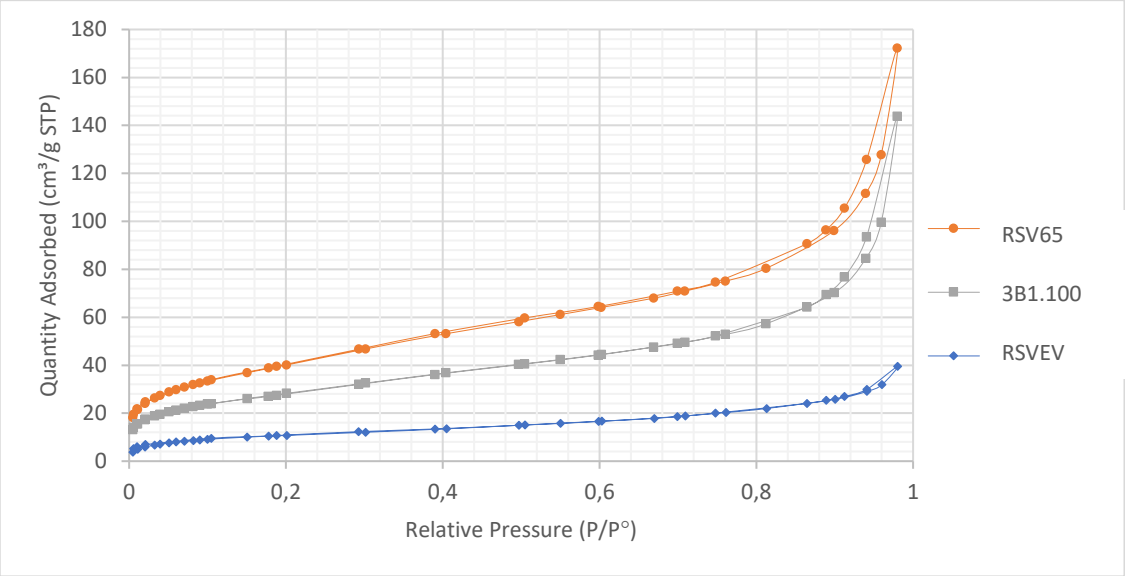

Figure 17 - N2 adsorption–desorption isotherms of sample 3B1.100 and loaded using the immersion and the evaporation methods.

The evaporation method was found to be by far the most adequate method for loading RSV in MSNs, considering the conditions used in these experiments. Rotary evaporation came as an effective method for loading RSV into the MSN, for this reason the method was used to proceed with the studies of loading and release. On the other hand, considering all the results relatively to the immersion method, the lack of characteristic bands of RSV in the FTIR, the TGA giving a weight similar to the unloaded NPs, and last the BET analysis it is reasonable to state that there is no evidence of the presence of RSV in the sample RSV65 and so the immersion method, with the tested conditions, is not effective for the loading of RSV in MSNs.

2.2 Loading efficiency and capacity

Sample 7B6.100 was the one chosen to proceed with the studies and test two different loading percentages, this sample was the selected due to is textural properties given by BET and STEM analysis. MSNs were loaded in the rotary evaporator using initial amounts of RSV of 40 and 80 mg (samples 7.40 and 7.80, respectively), with the aim of further evaluate differences in physicochemical properties and release profile. TGA was employed to calculate the percentage in mass of RSV present in the samples and results are present in Figure 18.

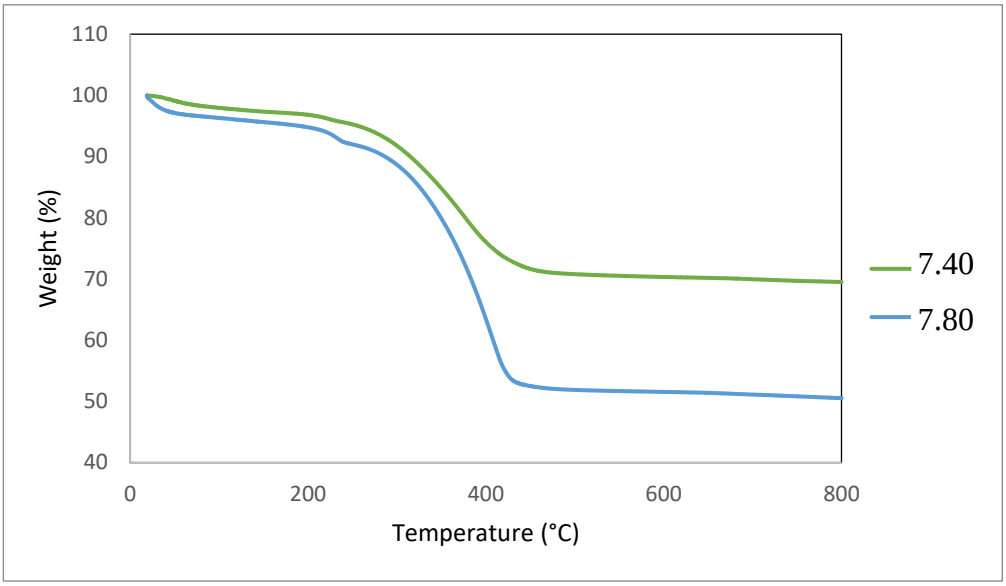

Figure 18 - TGA curve of loaded samples 7.40 and 7.80.

Considering weight losses from 200 to 700 ºC samples 7.40 and 7.80 had a weight loss of 26.8% and 43.7% respectively. This weight loss corresponds to the loading capacity. The loading efficiency was calculated using Equation 2.

$$Loading\ efficiency = \frac{m_{loaded\ RSV}}{m_{inicial\ RSV}} \times 100\% \quad (2)$$

In 7.40 40 mg of RSV and 100 mg of NPs were used, if all RSV had loaded onto the NPs the percentage of RSV in this sample would be 28.6%, so 93.7% of the RSV used in the loading experiment was probably loaded into the NPs. In the case of sample 7.80, 98.1% of the RSV used is present in the final material obtained after the loading experiment. The values of loading capacity and loading efficiency are summarized in the Table 4. Briefly, as

expected, it was observed that increasing the initial concentration of RSV leads to an increase of the loading capacity and loading efficiency.

Table 4 - Loading capacity and efficiency of samples 7.40 and 7.80.

Sample	Loading capacity (%)	Loading efficiency (%)
7.40	26.8	93.7
7.80	43.7	98.1

2.3 Characterization of RSV loaded MSNs

The samples 7.40 and 7.80 were further characterized using other techniques aiming to understand how RSV was loaded on the MSNs. During the loading process by evaporation, RSV molecules can be accommodated inside the pores or adsorbed at the surface of MSNs. Furthermore, it is possible that some of RSV molecules are free, i.e., with no interaction with MSNs.

The chemical composition of MSNs and loaded samples was investigated by elemental analysis and results are displayed in Table 5. The amount of carbon in MSNs is almost none, confirming the success of surfactant removal by wash and calcination. In this sample there is a small percentage of hydrogen probably prevenient from silanol groups and maybe from water molecules adsorbed to the surface of MSNs. For loaded samples percentages of carbon and hydrogen agree with the TGA results, both elements are present in the same proportion in each sample (approximately 62% for carbon and 63% for hydrogen) which is in agreement whit the proportion of total RSV wt% (approximately 65%)

Table 5 - Elemental analysis of MSNs and samples 7.40 and 7.80.

	MSNs	**7.40**	**7.80**
%C	0.040	20.208	32.472
%H	1.424	2.405	2.915

Thermograms from Figure 19 were obtained performing differential scanning calorimetry for samples 7.40, 7.80, MSNs and free RSV. Pure RSV presented a sharp

endothermic peak at 263.5 ºC that is attributed to the melting point of crystalline RSV. In the loaded sample such peak shifts for lower temperatures and suffer an intensity reduction, suggesting that RSV was in a non-crystalline form and therefore indicating the success of the loading process. Sample 7.40 is the one revealing a more amorphous state since the endothermic peak shifted for a lower temperature and the intensity of the peak decreased the most [103]. Solvent endothermic peaks were not present in any thermogram showing the successful removing of organic solvents of all samples [6], [104].

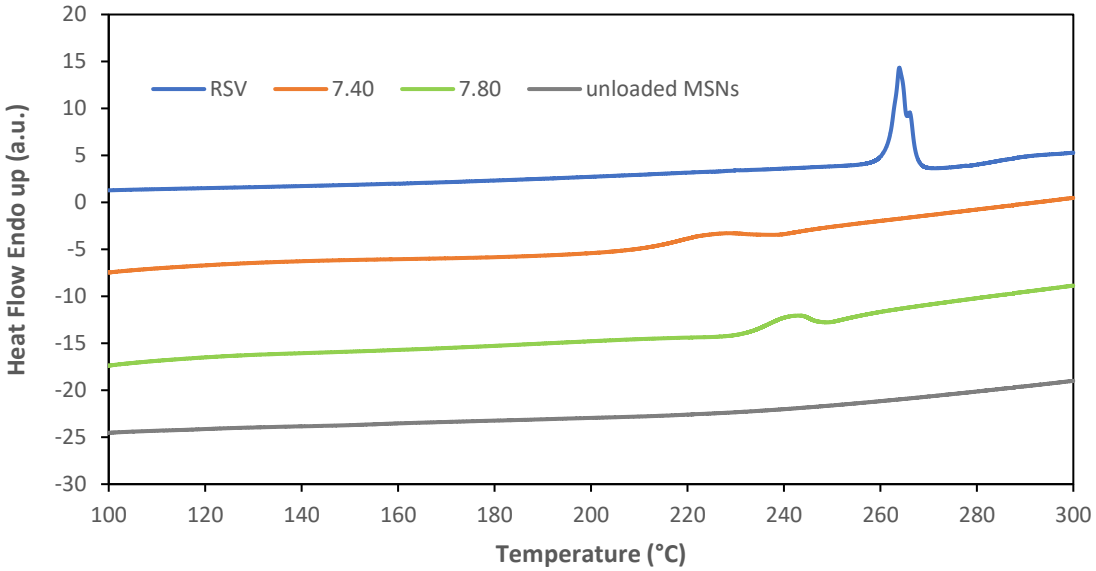

Figure 19 – Differential scanning calorimetry (DSC) curves of loaded samples 7.40 and 7.80, calcinated MSNs and pure RSV.

X-ray diffractogram of RSV exhibit multiple sharp peaks between 10 and 30°, this is due to the crystallinity of RSV when in its free form. When immobilized inside the pores drugs tend to change the structure of the organic entity from crystalline to amorphous [76]. Comparing free RSV with diffractograms of the loaded samples, it is clear that intensity of the peaks drops significantly, indicating that RSV is not completely in is crystalline form, tending to be in an amorphous state within the NPs [6]. 7.80 is the sample with the higher amount of RSV, approximately 43.7%, and also the one with more intense RSV peaks when compared to sample 7.40. In the diffractogram of 7.80 is clearly visible a peak of RSV near 24º (blue band of Figure 20) that is no visible in the diffractogram of 7.40. These results were expected and reveal that the amount of crystalline RSV is higher in 7.80 than in 7.40, probably free RSV in the surroundings of the NPs, which is in agreement with DSC results that also attribute lower crystallinity of RSV to sample 7.40. It was previously reported that

MSNs with larger pores allow crystallization of RSV inside the pores. The pore size of these NPs is 9.4 nm (BET results) and the ones reported in the literature were 7.0 nm, [76] which indicates that diffractograms of the loaded materials may have the contributions not only from free RSV in the surroundings of the NPs but also from crystalline RSV inside the mesopores. The broad peak of the MSNs suffer a decrease in intensity after loading, phenomenon that may be explained by the scattering effect of RSV filling the mesopores [100].

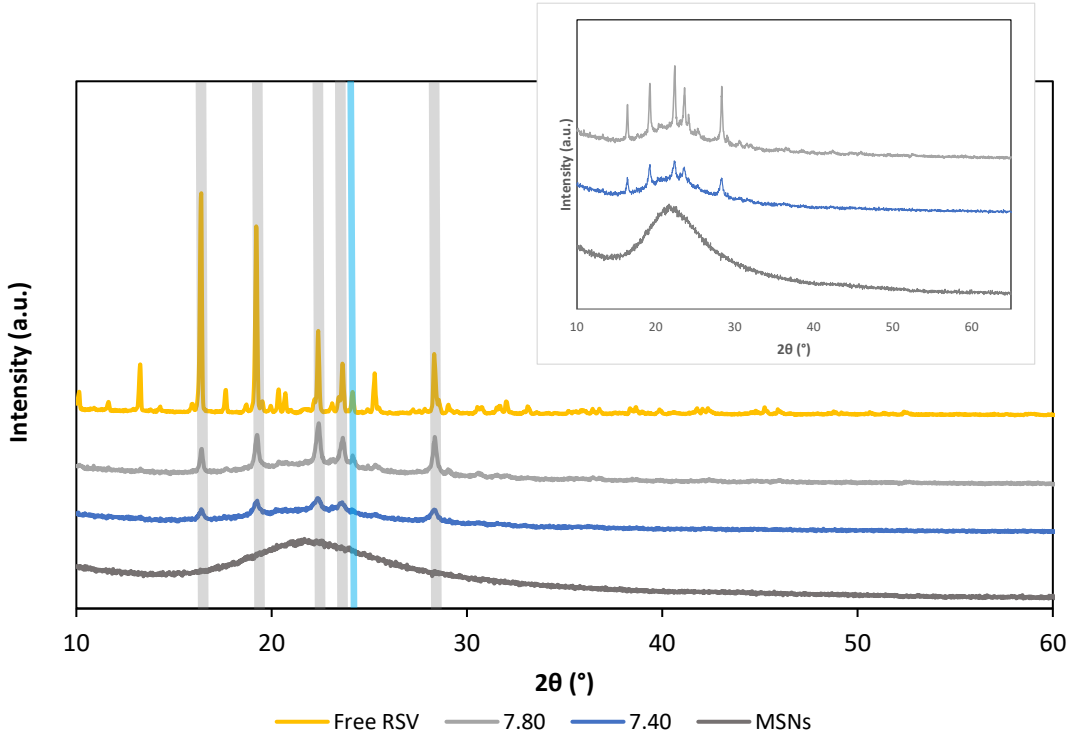

Figure 20- Wide angle XRD pattern of free RSV (Free RSV), MSNs and loaded samples 7.40 and 7.80.

The surface charge of the loaded NPs was assessed through measurement of zeta potential at variable pH value. However, the Zeta potential measurements of the loaded samples revealed a profile similar to the unloaded NPs, through the pH scale (Figure 21). The loaded particles presented zeta potential values below -30 mV for a wide range of pH values, above pH 4. These results indicate colloidal stability, including at the pH values used in this work for drug release (7.4 and 5.2).

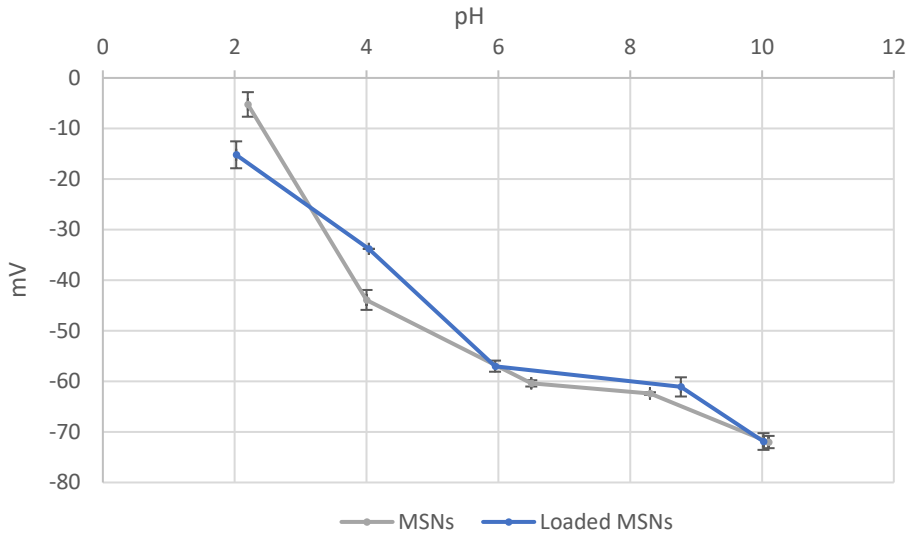

Figure 21 - Zeta potential of unloaded and loaded NPs at different pH values.

3. In vitro release studies

In vitro release studies were performed with samples 7.40 and 7.80, also free RSV was evaluated in order to compare with the loaded materials. The release tests were made under the same conditions but at two different pH values, 7.4 (physiological pH) and 5.2 that mimics the acid environment in some tumorous tissues. Results are shown in Figure 22.

For all samples including free RSV the release was faster under acidic conditions although, without any burst effect. In the first 24h at pH 5.2 cumulative release of RSV was 70.5%, 71.1% and 45.6% for samples 7.40, 7.80 and free RSV, respectively. Under more neutral pH conditions, for the same period of time, cumulative release decreased to 62.5%, 52.7% and 29.6% for samples 7.40, 7.80 and free RSV, respectively. Previous studies reported that RSV solubility is higher for lower pH values, and also acidic solutions of RSV are more stable than solutions with higher pH values [105]. Solubility may be the cause of the faster release of RSV under acidic conditions. Stability of RSV may also influence the release and the detection of RSV molecules.

After 72h, pH seems not to have a significant role in the cumulative released once it was similar for both pH values. However, as expected by parallelism with previous studies, it is clear that loaded samples reached higher release percentages when compared to free

RSV [6], [76]. Highlighting sample 7.40 has the one with highest cumulative release percentage, 97.5% for pH 7.4 and 105% for pH 5.2. The enhanced solubility of RSV may be attributed to the confined molecules of RSV in an amorphous state within the mesopores likewise the higher surface area of the MSNs providing higher diffusion rates [6].

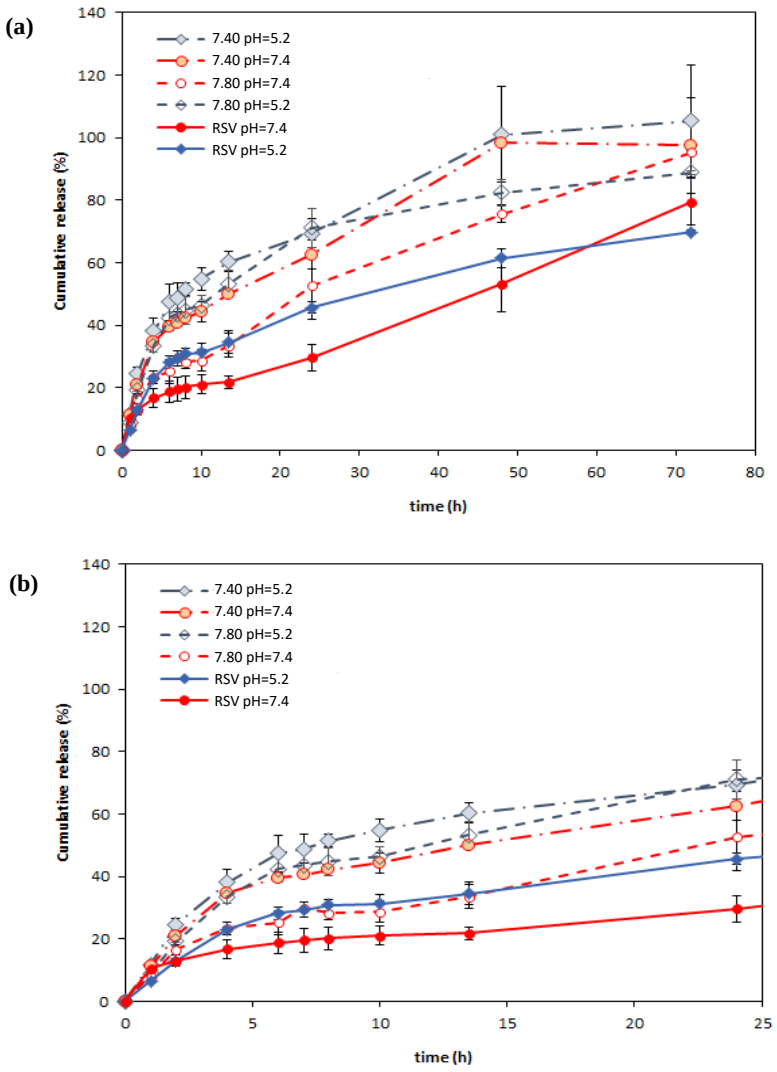

Figure 22 – Release profiles during (a) 72h and (b) 24h of loaded samples 7.40 and 7.80 as well as pure RSV.

Sample 7.40 seems to be the most effective RSV-MSNs system once it reaches higher release percentages requiring a lower quantity of RSV when compared to sample 7.80. This happens probably due to the different states in which the RSV molecules are in both samples. DRX results indicate that 7.80 has a higher amount of RSV in a crystalline form, comparing to 7.40, probably in the surroundings of the NPs, making harder the solubility and diffusion of RSV molecules in this sample.

IV. Conclusion

The synthesis method used in this work permitted to synthesize mesoporous silica NPs with different properties varying reaction conditions. Conditions that appeared to give better textural properties are 6 hours of synthesis and using 100 µL of TEA. NPs synthesized under these conditions were chosen to load with RSV and proceed to *in vitro* release studies.

In this work RSV was successfully encapsulated in MSNs using the rotary evaporation technique achieving good loading efficiency, above 90%. On the other hand, the also tested immersion method did not present comparable loading capacity.

The release profile of RSV from the MSNs was studied at different pH conditions. It was observed that in acidic conditions the release of RSV is slightly faster than it is in physiological pH conditions, however after 72h pH does not seem to affect much the cumulative release of RSV. Encapsulated RSV solubilizes easier in water than free RSV which is a very important feature of MSNs. The results of drug dissolution studies are in agreement with previous results reported in the literature.

Future work

RSV is a versatile molecule that can be applied in several field from food application, through cosmetics until biomedical applications, as well as MSNs which applicability in various contexts has been proven in the last years. These gives rise to the synthesised systems to be studied in many ways with different purposes. As a future work, it is proposed to evaluate the results of the cellular tests being carried out at this moment. Once RSV is well known for its antioxidant properties, and the systems as the capacity to enhance RSV solubility in aqueous environments, it would be interesting to evaluate the antioxidant activity of the systems. There are numerous antioxidant tests available, among them the $ABTS^{+}$ and DPPH, commonly used to assess the antioxidant activity of nutraceuticals.

With regard to the characterization of the nanoconjugate, NMR tests could be performed in other to better understand the molecular accommodation of RSV in the pores of both systems.

Coordination chemistry could also give interesting results to this study. Attempt to synthetize metal-resveratrol coordination compounds, besides RSV, copper and nickel, could be used as metal cores, and N-donor ligands such as 1,10-phenantroline, 2,2'-bipyrine, etc. After that, attempts would be made to load the synthesized metal complexes on MSNs, and further characterization, evaluation of the release profile and eventually biological tests.

Another approach could be loading of RSV together with a well-known anticancer drug, followed by the evaluation of the synergetic effect.

References

[1] D. Arora and S. Jaglan, "Nanocarriers based delivery of nutraceuticals for cancer prevention and treatment: A review of recent research developments," *Trends Food Sci. Technol.*, vol. 54, pp. 114–126, 2016.

[2] M. Yao, D. J. McClements, and H. Xiao, "Improving oral bioavailability of nutraceuticals by engineered nanoparticle-based delivery systems," *Curr. Opin. Food Sci.*, vol. 2, pp. 14–19, 2015.

[3] A. Nkondjock, P. Ghadirian, K. C. Johnson, and D. Krewski, "Dietary Intake of Lycopene Is Associated with Reduced Pancreatic Cancer Risk," *J. Nutr.*, vol. 135, no. 3, pp. 592–597, 2005.

[4] D. J. Mcclements, F. Li, and H. Xiao, "The Nutraceutical Bioavailability Classification Scheme : Classifying Nutraceuticals According to Factors Limiting their Oral Bioavailability," *Foof Sci. Technol.*, vol. 6, pp. 299–329, 2015.

[5] Y. Shen, B. Cao, N. R. Snyder, K. M. Woeppel, J. R. Eles, and X. T. Cui, "ROS responsive resveratrol delivery from LDLR peptide conjugated PLA-coated mesoporous silica nanoparticles across the blood-brain barrier," *J. Nanobiotechnology*, vol. 16, no. 1, pp. 1–17, 2018.

[6] N. Summerlin *et al.*, "Colloidal mesoporous silica nanoparticles enhance the biological activity of resveratrol," *Colloids Surfaces B Biointerfaces*, vol. 144, pp. 1–7, 2016.

[7] S. D. Rege, T. Geetha, G. D. Griffin, T. L. Broderick, and J. R. Babu, "Neuroprotective effects of resveratrol in Alzheimer disease pathology," *Front. Aging Neurosci.*, vol. 6, no. AUG, pp. 1–27, 2014.

[8] J. A. McCubrey *et al.*, "Effects of berberine, curcumin, resveratrol alone and in combination with chemotherapeutic drugs and signal transduction inhibitors on cancer cells—Power of nutraceuticals," *Adv. Biol. Regul.*, vol. 67, no. September 2017, pp. 190–211, 2018.

[9] A. C. Santos *et al.*, "Nanocarriers for resveratrol delivery: Impact on stability and solubility concerns," *Trends Food Sci. Technol.*, vol. 91, no. July, pp. 483–497, 2019.

[10] G. J. Soleas, E. P. Diamandis, and D. M. Goldberg, "Resveratrol: A molecule whose time has come? And gone?," *Clin. Biochem.*, vol. 30, no. 2, pp. 91–113, 1997.

[11] A. R. Neves, M. Lucio, J. L.C. Lima, and S. Reis, "Resveratrol in Medicinal Chemistry: A Critical Review of its Pharmacokinetics, Drug-Delivery, and Membrane Interactions," *Curr.*

Med. Chem., vol. 19, no. 11, pp. 1663–1681, 2012.

[12] X. Sun, Y. Shao, and W. Yan, "Measurement and correlation of solubilities of irans-resveratrol in ethanol + water and acetone + water mixed solvents at different temperatures," *J. Chem. Eng. Data*, vol. 53, no. 11, pp. 2562–2566, 2008.

[13] Q. Xu *et al.*, "Resveratrol in the treatment of pancreatic cancer," *Ann. N. Y. Acad. Sci.*, vol. 1348, no. 1, pp. 10–19, 2015.

[14] D. G. Zayed *et al.*, "Combining hydrophilic chemotherapy and hydrophobic phytotherapy via tumor-targeted albumin-QDs nano-hybrids: Covalent coupling and phospholipid complexation approaches," *J. Nanobiotechnology*, vol. 17, no. 1, pp. 1–19, 2019.

[15] S. Das, H. S. Lin, P. C. Ho, and K. Y. Ng, "The impact of aqueous solubility and dose on the pharmacokinetic profiles of resveratrol," *Pharm. Res.*, vol. 25, no. 11, pp. 2593–2600, 2008.

[16] A. Z. Wang, R. Langer, and O. C. Farokhzad, "Nanoparticle Delivery of Cancer Drugs," *Annu. Rev. Med.*, vol. 63, no. 1, pp. 185–198, Feb. 2012.

[17] R. Narayan, U. Y. Nayak, A. M. Raichur, and S. Garg, "Mesoporous silica nanoparticles: A comprehensive review on synthesis and recent advances," *Pharmaceutics*, vol. 10, no. 3, pp. 1–49, 2018.

[18] M. R. Díaz and P. E. Vivas-Mejia, "Nanoparticles as drug delivery systems in cancer medicine: Emphasis on RNAi-containing nanoliposomes," *Pharmaceuticals*, vol. 6, no. 11, pp. 1361–1380, 2013.

[19] A. Kumari, S. K. Yadav, and S. C. Yadav, "Biodegradable polymeric nanoparticles based drug delivery systems," *Colloids Surfaces B Biointerfaces*, vol. 75, no. 1, pp. 1–18, 2010.

[20] D. Arora, N. Sharma, V. Sharma, V. Abrol, R. Shankar, and S. Jaglan, "An update on polysaccharide-based nanomaterials for antimicrobial applications," *Appl. Microbiol. Biotechnol.*, vol. 100, no. 6, pp. 2603–2615, 2016.

[21] X. Liu, B. Zhang, I. S. Sohal, D. Bello, and H. Chen, *Is "nano safe to eat or not"? A review of the state-of-the art in soft engineered nanoparticle (sENP) formulation and delivery in foods*, 1st ed., vol. 88. Elsevier Inc., 2019.

[22] I. Khan, K. Saeed, and I. Khan, "Nanoparticles: Properties, applications and toxicities," *Arab. J. Chem.*, vol. 12, no. 7, pp. 908–931, 2019.

[23] M. Bamburowicz-Klimkowska, M. Poplawska, and I. P. Grudzinski, *Nanocomposites as biomolecules delivery agents in nanomedicine*, vol. 17, no. 1. BioMed Central, 2019.

[24] L. Q. Zou *et al.*, "Improved in vitro digestion stability of (-)-epigallocatechin gallate through nanoliposome encapsulation," *Food Res. Int.*, vol. 64, pp. 492–499, 2014.

[25] FDA, "Food Additive Status List," 2019. [Online]. Available: https://www.fda.gov/food/food-additives-petitions/food-additive-status-list.

[26] P. Ramalingam and Y. T. Ko, “Improved oral delivery of resveratrol from N-trimethyl chitosan-g-palmitic acid surface-modified solid lipid nanoparticles,” *Colloids Surfaces B Biointerfaces*, vol. 139, pp. 52–61, 2016.

[27] E. Soo, S. Thakur, Z. Qu, S. Jambhrunkar, H. S. Parekh, and A. Popat, “Enhancing delivery and cytotoxicity of resveratrol through a dual nanoencapsulation approach,” *J. Colloid Interface Sci.*, vol. 462, pp. 368–374, 2016.

[28] J. Tang *et al.*, “Poly(lactic acid)-coated mesoporous silica nanosphere for controlled release of venlafaxine,” *J. Colloid Interface Sci.*, vol. 360, no. 2, pp. 488–496, 2011.

[29] Z. Chaudhary *et al.*, “Encapsulation and Controlled Release of Resveratrol Within Functionalized Mesoporous Silica Nanoparticles for Prostate Cancer Therapy,” *Front. Bioeng. Biotechnol.*, vol. 7, no. September, pp. 1–9, 2019.

[30] T. S. Anirudhan and A. S. Nair, “Temperature and ultrasound sensitive gatekeepers for the controlled release of chemotherapeutic drugs from mesoporous silica nanoparticles,” *J. Mater. Chem. B*, vol. 6, no. 3, pp. 428–439, 2018.

[31] A. Maleki, H. Kettiger, A. Schoubben, J. M. Rosenholm, V. Ambrogi, and M. Hamidi, “Mesoporous silica materials: From physico-chemical properties to enhanced dissolution of poorly water-soluble drugs,” *J. Control. Release*, vol. 262, no. June, pp. 329–347, 2017.

[32] A. Galarneau, H. Cambon, F. Di Renzo, R. Ryoo, M. Choi, and F. Fajula, “Microporosity and connections between pores in SBA-15 mesostructured silicas as a function of the temperature of synthesis,” *New J. Chem.*, vol. 27, no. 1, pp. 73–79, 2003.

[33] Z. Yi *et al.*, “A New Insight into Growth Mechanism and Kinetics of Mesoporous Silica Nanoparticles by in Situ Small Angle X-ray Scattering,” *Langmuir*, vol. 31, no. 30, pp. 8478–8487, 2015.

[34] N. A. Zainal, S. R. A. Shukor, H. A. A. Wab, and K. A. Razak, “Study on the effect of synthesis parameters of silica nanoparticles entrapped with rifampicin,” *Chem. Eng. Trans.*, vol. 32, pp. 2245–2250, 2013.

[35] X. Huang, X. Teng, D. Chen, F. Tang, and J. He, “The effect of the shape of mesoporous silica nanoparticles on cellular uptake and cell function,” *Biomaterials*, vol. 31, no. 3, pp. 438–448, 2010.

[36] L. Ding and B. Su, “An electrochemistry assisted approach for fast, low-cost and gram-scale synthesis of mesoporous silica nanoparticles,” *RSC Adv.*, vol. 5, no. 81, pp. 65922–65926, 2015.

[37] S. Bian, K. Gao, H. Shen, X. Jiang, Y. Long, and Y. Chen, “Organic/inorganic hybrid mesoporous silica membrane rapidly synthesized by a microwave-assisted method and its application in enzyme adsorption and electrocatalysis,” *J. Mater. Chem. B*, vol. 1, no. 26, pp.

3267–3276, 2013.

[38] Y. Snoussi, S. Bastide, M. Abderrabba, and M. M. Chehimi, “Sonochemical synthesis of Fe3O4@NH2-mesoporous silica@Polypyrrole/Pd: A core/double shell nanocomposite for catalytic applications,” *Ultrason. Sonochem.*, vol. 41, no. September 2017, pp. 551–561, 2018.

[39] A. I. Akinjokun, T. V Ojumu, and A. O. Ogunfowokan, “Biomass, Abundant Resources for Synthesis of Mesoporous Silica Material,” in *Intech*, 2016, pp. 103–117.

[40] A. Mourhly, M. Khachani, A. El Hamidi, M. Kacimi, M. Halim, and S. Arsalane, “The synthesis and characterization of low-cost mesoporous silica SiO2 from local pumice rock,” *Nanomater. Nanotechnol.*, vol. 5, 2015.

[41] P. Parhi, C. Mohanty, and S. K. Sahoo, “Nanotechnology-based combinational drug delivery : an emerging approach for cancer therapy,” *Drug Discov. Today*, vol. 17, no. 17–18, pp. 1044–1052, 2012.

[42] P. Soni, J. Kaur, and K. Tikoo, “Dual drug-loaded paclitaxel–thymoquinone nanoparticles for effective breast cancer therapy,” *Joarnal Nanoparticle Res.*, vol. 17, no. 1, p. 18, 2015.

[43] A. M. Chen *et al.*, “Co-delivery of Doxorubicin and Bcl-2 siRNA by Mesoporous Silica Nanoparticles Enhances the Efficacy of Chemotherapy in Multidrug-Resistant Cancer Cells **,” *Small*, vol. 23, pp. 2673–2677, 2009.

[44] X. Wang, P. Wang, Y. Jiang, Q. Su, and J. Zheng, “Facile surface modification of silica nanoparticles with a combination of noncovalent and covalent methods for composites application,” *Compos. Sci. Technol.*, vol. 104, pp. 1–8, 2014.

[45] A. Liberman, N. Mendez, W. C. Trogler, and A. C. Kummel, “Synthesis and surface functionalization of silica nanoparticles for nanomedicine,” *Surf. Sci. Rep.*, vol. 69, no. 2–3, pp. 132–158, 2014.

[46] C. Lee, L. Lo, C. Yang, T. City, and C. Mou, “Charged mesoporous silica nanoparticle-based drug delivery system for controlled release and enhanced bioavailability,” US 2010/0104650 A1, 2010.

[47] H. Nabeshi *et al.*, “Systemic distribution, nuclear entry and cytotoxicity of amorphous nanosilica following topical application,” *Biomaterials*, vol. 32, no. 11, pp. 2713–2724, 2011.

[48] W. I. Hagens, A. G. Oomen, W. H. De Jong, F. R. Cassee, and J. A. M. Sips, “What do we (need to) know about the kinetic properties of nanoparticles in the body?,” *Regul. Toxicol. Pharmacol.*, vol. 49, pp. 217–229, 2007.

[49] C. Fu, T. Liu, L. Li, H. Liu, D. Chen, and F. Tang, “The absorption, distribution, excretion and toxicity of mesoporous silica nanoparticles in mice following different exposure routes,” *Biomaterials*, vol. 34, no. 10, pp. 2565–2575, 2013.

[50] T. Liu *et al.*, “Single and repeated dose toxicity of mesoporous hollow silica nanoparticles in intravenously exposed mice,” *Biomaterials*, vol. 32, no. 6, pp. 1657–1668, 2011.

[51] F. J. Gutiérrez *et al.*, “Methods for the nanoencapsulation of β-carotene in the food sector,” *Trends Food Sci. Technol.*, vol. 32, no. 2, pp. 73–83, 2013.

[52] X. He and H. Hwang, “Nanotechnology in food science: Functionality, applicability, and safety assessment,” *J. Food Drug Anal.*, vol. 24, no. 4, pp. 671–681, 2016.

[53] N. Vaze *et al.*, “A nano-carrier platform for the targeted delivery of nature-inspired antimicrobials using Engineered Water Nanostructures for food safety applications,” *Food Control*, vol. 96, no. August 2018, pp. 365–374, 2019.

[54] A. Bernardos and L. Kouřimská, “Applications of Mesoporous Silica Materials in Food – a Review,” *Czech J. Food Sci.*, vol. 31, no. 2, pp. 99–107, 2013.

[55] S. Morante-zarcero, I. Sierra, and N. Casado, “Current development and applications of ordered mesoporous silicas and other sol e gel silica-based materials in food sample preparation for xenobiotics analysis n P e,” *Trends Anal. Chem.*, vol. 88, pp. 167–184, 2017.

[56] M. Coimbra *et al.*, “Improving solubility and chemical stability of natural compounds for medicinal use by incorporation into liposomes,” *Int. J. Pharm.*, vol. 416, no. 2, pp. 433–442, 2011.

[57] S. N. Park, N. R. Jo, and S. H. Jeon, “Chitosan-coated liposomes for enhanced skin permeation of resveratrol,” *J. Ind. Eng. Chem.*, vol. 20, no. 4, pp. 1481–1485, 2014.

[58] D. Cosco *et al.*, “Ultradeformable liposomes as multidrug carrier of resveratrol and 5-fluorouracil for their topical delivery,” *Int. J. Pharm.*, vol. 489, no. 1–2, pp. 1–10, 2015.

[59] M. Wenche, G. Acharya, and P. Basnet, “Resveratrol-loaded liposomes for topical treatment of the vaginal in fl ammation and infections,” *Eur. J. Pharm. Sci.*, vol. 79, pp. 112–121, 2015.

[60] C. Caddeo *et al.*, “Nanocarriers for antioxidant resveratrol: Formulation approach, vesicle self-assembly and stability evaluation,” *Colloids Surfaces B Biointerfaces*, vol. 111, pp. 327–332, 2013.

[61] V. Venuti *et al.*, “A characterization study of resveratrol/sulfobutyl ether-beta-cyclodextrin inclusion complex and in vitro anticancer activity,” *Colloids Surfaces B Biointerfaces*, vol. 115, pp. 22–28, 2014.

[62] Z. Lu, R. Chen, H. Liu, Y. Hu, B. Cheng, and G. Zou, “Study of the complexation of resveratrol with cyclodextrins by spectroscopy and molecular modeling,” *J. Incl. Phenom. Macrocycl. Chem.*, vol. 63, no. 3–4, pp. 295–300, 2009.

[63] M. E. Carlotti *et al.*, “Resveratrol in Solid Lipid Nanoparticles,” *J. Dispers. Sci. Techology*, vol. 33, pp. 465–471, 2012.

[64] E. H. Gokce, E. Korkmaz, E. Dellera, M. C. Bonferoni, and O. Ozer, “Resveratrol-loaded

solid lipid nanoparticles versus nanostructured lipid carriers : evaluation of antioxidant potential for dermal applications," *Int. J. Nanomedicine*, vol. 7, pp. 1841–1850, 2012.

[65] S. Jose, S. S. Anju, T. A. Cinu, N. A. Aleykutty, S. Thomas, and E. B. Souto, "In vivo pharmacokinetics and biodistribution of resveratrol-loaded solid lipid nanoparticles for brain delivery," *Int. J. Pharm.*, vol. 474, no. 1–2, pp. 6–13, 2014.

[66] X. Lu *et al.*, "Resveratrol-loaded polymeric micelles protect cells from AB-induced oxidative stress," *Int. J. Pharm.*, vol. 375, pp. 89–96, 2009.

[67] B. Cote, L. Janssen, D. A. Rao, and A. W. G. Alani, "Combinatorial resveratrol and quercetin polymeric micelles mitigate doxorubicin induced cardiotoxicity in vitro and in vivo," *J. Control. Release*, vol. 213, pp. 128–133, 2015.

[68] Y. O. Jeon, J. Lee, and H. G. Lee, "Improving solubility , stability , and cellular uptake of resveratrol by nanoencapsulation with chitosan and γ -poly (glutamic acid)," *Colloids Surfaces B Biointerfaces*, vol. 147, pp. 224–233, 2016.

[69] B. Carletto *et al.*, "Resveratrol-loaded nanocapsules inhibit murine melanoma tumor growth," *Colloids Surfaces B Biointerfaces*, vol. 144, pp. 65–72, 2016.

[70] U. M. Musazzi, I. Youm, J. B. Murowchick, M. J. Ezoulin, and B. C. Youan, "Colloids and Surfaces B : Biointerfaces Resveratrol-loaded nanocarriers : Formulation , optimization , characterization and in vitro toxicity on cochlear cells," *Colloids Surfaces B Biointerfaces*, vol. 118, pp. 234–242, 2014.

[71] S. Karthikeyan, N. R. Prasad, A. Ganamani, and E. Balamurugan, "Anticancer activity of resveratrol-loaded gelatin nanoparticles on NCI-H460 non-small cell lung cancer cells," *Biomed. Prev. Nutr.*, vol. 3, no. 1, pp. 64–73, 2013.

[72] C. Tsai, J. L. Vivero-escoto, I. I. Slowing, I. Fang, B. G. Trewyn, and V. S. Lin, "Biomaterials Surfactant-assisted controlled release of hydrophobic drugs using anionic surfactant templated mesoporous silica nanoparticles," *Biomaterials*, vol. 32, no. 26, pp. 6234–6244, 2011.

[73] V. V Cotea, C. E. Luchian, N. Bilba, and M. Niculaua, "Analytica Chimica Acta Mesoporous silica SBA-15, a new adsorbent for bioactive polyphenols from red wine," *Anal. Chim. Acta*, vol. 732, pp. 180–185, 2012.

[74] M. Popova *et al.*, "Preparation of resveratrol-loaded nanoporous silica materials with different structures," *J. Solid State Chem.*, vol. 219, pp. 37–42, 2014.

[75] R. Zhang, G. Wang, J. Xu, Y. Tu, Y. Yang, and F. Li, "Preparation and evaluation of resveratrol-loaded mesoporous silica nanoparticles modified by amino," *Chinese Pharm. J.*, vol. 50, no. 5, pp. 413–419, 2015.

[76] E. Juère *et al.*, "In Vitro Dissolution, Cellular Membrane Permeability, and Anti-

Inflammatory Response of Resveratrol-Encapsulated Mesoporous Silica Nanoparticles," *Mol. Pharm.*, vol. 14, pp. 4431–4441, 2017.

[77] Y. Hu, Z. Wang, Y. Qiu, Y. Liu, M. Ding, and Y. Zhang, "Anti-miRNA21 and resveratrol-loaded polysaccharide-based mesoporous silica nanoparticle for synergistic activity in gastric carcinoma," *J. Drug Target.*, pp. 1135–1143, 2019.

[78] L. Pan *et al.*, "Nuclear-targeted drug delivery of tat peptide-conjugated monodisperse mesoporous silica nanoparticles," *J. Am. Chem. Soc.*, vol. 134, no. 13, pp. 5722–5725, 2012.

[79] G. Quan *et al.*, "Lactosaminated mesoporous silica nanoparticles for asialoglycoprotein receptor targeted anticancer drug delivery," *J. Nanobiotechnology*, vol. 13, no. 1, pp. 1–12, 2015.

[80] N. H. N. Kamarudin *et al.*, "Role of 3-aminopropyltriethoxysilane in the preparation of mesoporous silica nanoparticles for ibuprofen delivery: Effect on physicochemical properties," *Microporous Mesoporous Mater.*, vol. 180, pp. 235–241, 2013.

[81] K. S. W. Sing, "Reporting physisorption data for gas/solid systems," *Pure Appl. Chem.*, vol. 54, no. 11, pp. 2201–2218, 1982.

[82] M. Mohseni, K. Gilani, and S. A. Mortazavi, "Preparation and characterization of rifampin loaded mesoporous silica nanoparticles as a potential system for pulmonary drug delivery," *Iran. J. Pharm. Res.*, vol. 14, no. 1, pp. 27–34, 2015.

[83] M. Thommes *et al.*, "Physisorption of gases, with special reference to the evaluation of surface area and pore size distribution (IUPAC Technical Report)," 2015.

[84] V. Cauda, A. Schlossbauer, and T. Bein, "Bio-degradation study of colloidal mesoporous silica nanoparticles: Effect of surface functionalization with organo-silanes and poly(ethylene glycol)," *Microporous Mesoporous Mater.*, vol. 132, no. 1–2, pp. 60–71, 2010.

[85] M. Manzano *et al.*, "Studies on MCM-41 mesoporous silica for drug delivery: Effect of particle morphology and amine functionalization," *Chem. Eng. J.*, vol. 137, no. 1, pp. 30–37, 2008.

[86] A. Ganguly, T. Ahmad, and A. K. Ganguli, "Silica mesostructures: Control of pore size and surface area using a surfactant-templated hydrothermal process," *Langmuir*, vol. 26, no. 18, pp. 14901–14908, 2010.

[87] F. J. Sotomayor, K. A. Cychosz, and M. Thommes, "Characterization of Micro/Mesoporous Materials by Physisorption: Concepts and Case Studies," *Acc. Mater. Surf. Res*, vol. 3, no. 2, pp. 34–50, 2018.

[88] D. Tang, W. Zhang, Y. Zhang, Z. Qiao, Y. Liu, and Q. Huo, "Journal of Colloid and Interface Science Transition metal complexes on mesoporous silica nanoparticles as highly efficient catalysts for epoxidation of styrene," *J. Colloid Interface Sci.*, vol. 356, no. 1, pp. 262–266,

2011.

[89] Y. Zhang, Z. Zhi, T. Jiang, J. Zhang, Z. Wang, and S. Wang, “Spherical mesoporous silica nanoparticles for loading and release of the poorly water-soluble drug telmisartan,” *J. Control. Release*, vol. 145, no. 3, pp. 257–263, 2010.

[90] S. Bhattacharjee, “DLS and zeta potential - What they are and what they are not?,” *J. Control. Release*, vol. 235, pp. 337–351, 2016.

[91] K. E.A. AbouAitah and A. A. Farghali, “Mesoporous Silica Materials in Drug Delivery System: pH/Glutathione- Responsive Release of Poorly Water-Soluble Pro-drug Quercetin from Two and Three-dimensional Pore-Structure Nanoparticles,” *J. Nanomed. Nanotechnol.*, vol. 07, no. 02, 2016.

[92] A. Neumann, A. Christel, C. Kasper, and P. Behrens, “BMP2-loaded nanoporous silica nanoparticles promote osteogenic differentiation of human mesenchymal stem cells,” *RSC Adv.*, vol. 3, no. 46, pp. 24222–24230, 2013.

[93] A. M. Basso, B. P. Nicola, K. Bernardo-Gusmão, and S. B. C. Pergher, “Tunable effect of the calcination of the silanol groups of KIT-6 and SBA-15 mesoporous materials,” *Appl. Sci.*, vol. 10, no. 3, pp. 1–16, 2020.

[94] N. Schmidt *et al.*, “Long-term delivery of brain-derived neurotrophic factor (BDNF) from nanoporous silica nanoparticles improves the survival of spiral ganglion neurons in vitro,” *PLoS One*, vol. 13, no. 3, pp. 1–23, 2018.

[95] V. Selvamani, *Stability Studies on Nanomaterials Used in Drugs*. Elsevier Inc., 2018.

[96] V. L. Gaikwad, P. B. Choudhari, N. M. Bhatia, and M. S. Bhatia, *Characterization of pharmaceutical nanocarriers: In vitro and in vivo studies*. Elsevier Inc., 2019.

[97] E. Joseph and G. Singhvi, *Multifunctional nanocrystals for cancer therapy: A potential nanocarrier*. Elsevier Inc., 2019.

[98] K. Möller, J. Kobler, and T. Bein, “Colloidal suspensions of nanometer-sized mesoporous silica,” *Adv. Funct. Mater.*, vol. 17, no. 4, pp. 605–612, 2007.

[99] D. Kumar, K. Schumacher, C. Du Fresne von Hohenesche, M. Grün, and K. K. Unger, “MCM-41, MCM-48 and related mesoporous adsorbents: their synthesis and characterisation,” *Colloids Surfaces A Physicochem. Eng. Asp.*, vol. 187–188, pp. 109–116, 2001.

[100] S. Das, J. Manam, and S. K. Sharma, “Role of rhodamine-B dye encapsulated mesoporous SiO2 in color tuning of SrAl2O4:Eu2+,Dy3+ composite long lasting phosphor,” *J. Mater. Sci. Mater. Electron.*, vol. 27, no. 12, pp. 13217–13228, 2016.

[101] A. Gumireddy, R. Christman, D. Kumari, A. Tiwari, E. J. North, and H. Chauhan, “Preparation, Characterization, and In vitro Evaluation of Curcumin- and Resveratrol-Loaded

Solid Lipid Nanoparticles," *AAPS PharmSciTech*, vol. 20, no. 4, 2019.

[102] R. de C. da Silva *et al.*, "Resveratrol: A thermoanalytical study," *Food Chem.*, vol. 237, no. October, pp. 561–565, 2017.

[103] H. Abouhakim *et al.*, "Mechanically Induced Amorphization of Diaqua-bis(Omeprazolate)-Magnesium Dihydrate," *Cryst. Growth Des.*, vol. 20, pp. 6057–6068, 2020.

[104] S. Lungare, K. Hallam, and R. K. S. Badhan, "Phytochemical-loaded mesoporous silica nanoparticles for nose-to-brain olfactory drug delivery," *Int. J. Pharm.*, vol. 513, no. 1–2, pp. 280–293, 2016.

[105] Š. Zupančič, Z. Lavrič, and J. Kristl, "Stability and solubility of trans-resveratrol are strongly influenced by pH and temperature," *Eur. J. Pharm. Biopharm.*, vol. 93, pp. 196–204, 2015.

Supplementary material

Calibration curve for RSV

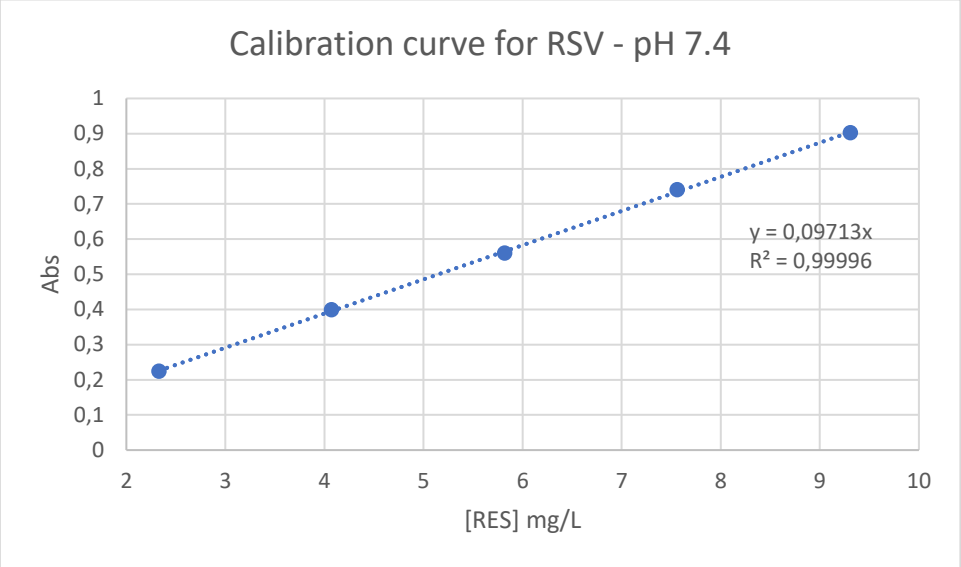

Figure 1sa - Calibrations curve for RSV in PBS pH 7.4.

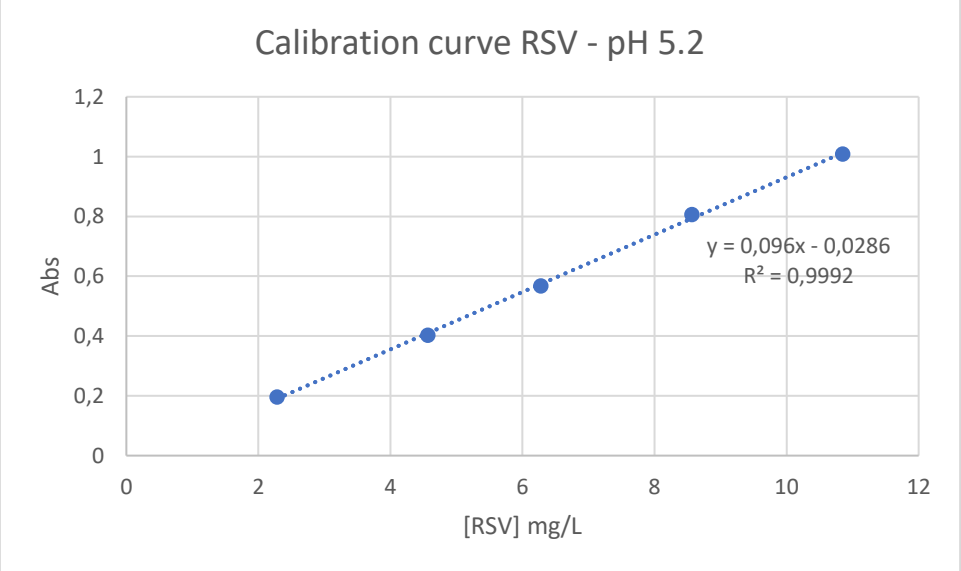

Figure 2sa - Calibration curve for RSV in PBS pH 5.2.

N_2 adsorption-desorption isotherm

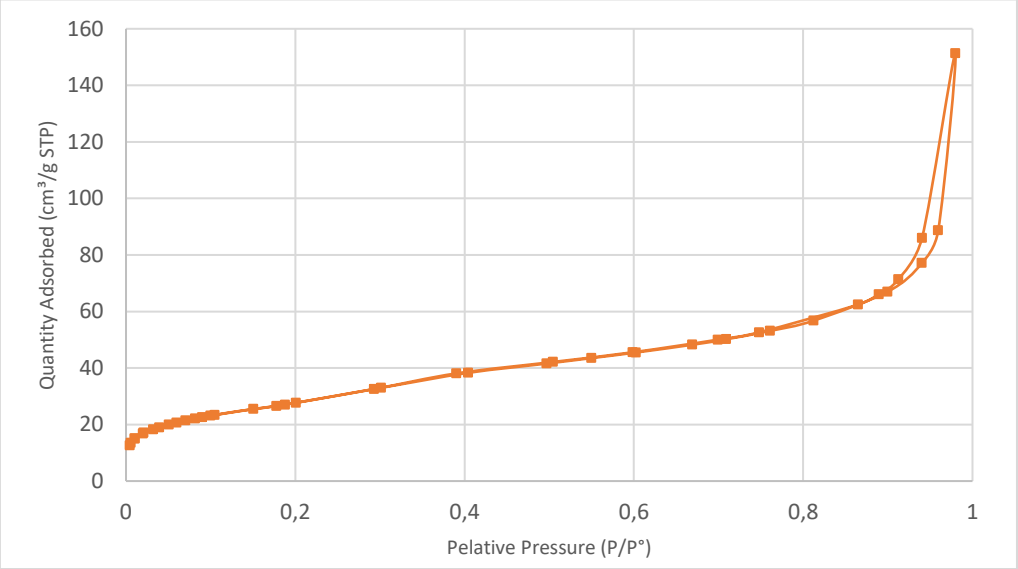

Figure 3sa - N_2 adsorption–desorption isotherms of sample 6B6.50.

RSV spectra

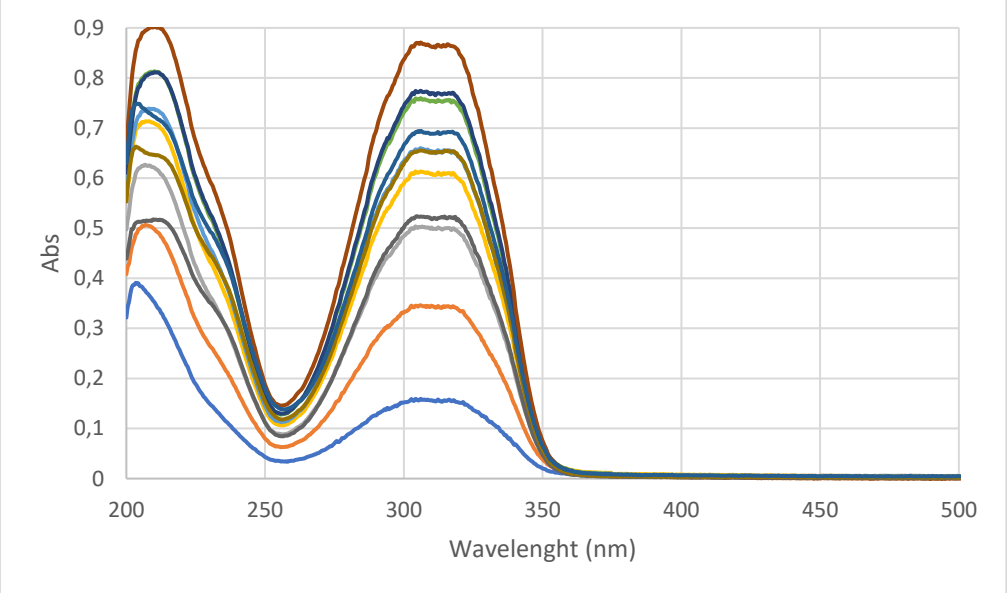

Figure 4sa – RSV spectra obtained at various times of sample 7.40 at pH 5.2.